Molecular Pharmacology Fast Forward. Published on August 16, 2007 as doi:10.1124/mol.107.034207

MiTMAB and OcTMAB are surface-active small molecule dynamin inhibitors that block endocytosis mediated by dynamin I or dynamin II

Annie Quan, Andrew B. McGeachie, Damien J. Keating, Ellen M. van Dam, Jenny Rusak, Ngoc Chau, Chandra S. Malladi, Chen Chen, Adam McCluskey, Michael A. Cousin, and Phillip J. Robinson

Cell Signalling Unit, Children's Medical Research Institute, The University of Sydney Locked Bag 23, Wentworthville, Sydney, NSW 2145, AUSTRALIA,
Tel: +61-2-9687-2800; Fax: +61-2-9687-2120
(A.Q., A.B.M., E.M.D., J.R., N.C., C.S.M., P.J.R.)

Chemistry, School of Environmental and Life Sciences, The University of Newcastle, Callaghan, NSW 2308, Australia (A.M.).
Department of Human Physiology, Flinders University, Adelaide, South Australia, 5001, Australia (D.J.K.).
Prince Henry's Institute of Medical Research, PO Box 5152, Clayton, Vic. 3168, Australia (C.C.).
Membrane Biology Group, Centre for Integrative Physiology, George Square, University of Edinburgh, Edinburgh, Scotland, UK, EH8 9XD (M.A.C).

Molecular Pharmacology Fast Forward. Published on August 16, 2007 as DOI: 10.1124/mol.107.034207
This article has not been copyedited and formatted. The final version may differ from this version.

Running Title Page:

Running title: Dynamin inhibitors MiTMAB and OcTMAB block endocytosis.

Corresponding author:
Phillip J. Robinson
Cell Signalling Unit,
Children's Medical Research Institute,
Locked Bag 23, Wentworthville,
Sydney, NSW 2145, AUSTRALIA,
Tel: +61-2-9687-2800
Fax: +61-2-9687-2120.
E-mail: probinson@cmri.com.au

The number of text pages:

Number of tables:	1
Number of figures:	6
Number of references:	40
Number of words in the Abstract:	188
Number of words in the Introduction:	722
Number of words in the Discussion:	1624

Nonstandard abbreviations:
DoTMAB, Dodecyl trimethyl ammonium bromide; MiTMAB, Myristyl trimethyl ammonium bromide; OcTMAB, Octadecyl trimethyl ammonium bromide;
EGF, epidermal growth factor;
GED, GTPase effector domain;
PH domain, pleckstrin homology domain;
PS, L-Phosphatidylserine;
PtdIns(4,5)P_2, phosphatidylinositol-4,5-bisphosphate;
PRD, proline-rich domain;
RME, receptor mediated endocytosis;
SVE, synaptic vesicle endocytosis;
Tf, transferrin;

Molecular Pharmacology Fast Forward. Published on August 16, 2007 as DOI: 10.1124/mol.107.034207
This article has not been copyedited and formatted. The final version may differ from this version.

ABSTRACT

Dynamin is a GTPase enzyme involved in membrane constriction and fission during endocytosis. Phospholipid binding via its pleckstrin homology (PH) domain maximally stimulates dynamin activity. We developed a series of surface-active small molecule inhibitors, such as myristyl trimethyl ammonium bromide (MiTMAB) and octadecyltrimethyl ammonium bromide (OcTMAB), and now show MiTMAB targets the dynamin-phospholipid interaction. MiTMAB inhibited dynamin GTPase activity with a K_i of 940 $\pm$ 25 nM. It potently inhibited receptor mediated endocytosis (RME) of transferrin or epidermal growth factor (EGF) in a range of cells without blocking EGF binding, receptor number or autophosphorylation. RME inhibition was rapidly reversed after washout. The rank order of potency for a variety of MiTMAB analogues on RME matched the rank order for dynamin inhibition, suggesting dynamin recruitment to the membrane is a primary cellular target. MiTMAB also inhibited synaptic vesicle endocytosis (SVE) in rat brain nerve terminals (synaptosomes) without inducing depolarization or morphological defects. Therefore the drug rapidly and reversibly blocks multiple forms of endocytosis with no acute cellular damage. MiTMAB's unique mechanism of action provides an important tool to better understand dynamin-mediated membrane trafficking events in a variety of cells.

Molecular Pharmacology Fast Forward. Published on August 16, 2007 as DOI: 10.1124/mol.107.034207
This article has not been copyedited and formatted. The final version may differ from this version.

INTRODUCTION

Endocytosis in eukaryotic cells services the uptake of extracellular material and the recycling of membrane components. Multiple forms of endocytosis exist which regulate a variety of different cellular processes, such as regulation of cell surface receptor expression and signalling, cell fate determination, cell migration, antigen presentation, and synaptic transmission (Liu and Robinson, 1995;Kaksonen *et al.*, 2006). Two of the best characterised pathways are receptor mediated endocytosis (RME) and synaptic vesicle endocytosis (SVE). Both utilize many proteins and lipid-cofactors (Cousin and Robinson, 2001;Le Roy and Wrana, 2005). RME is activated by binding of hormones or growth factor ligands to specific cell surface receptors, for example transferrin (Tf) and epidermal growth factor (EGF). RME usually occurs via clathrin-coated pits and requires the ubiquitously expressed GTPase dynamin II (Trowbridge *et al.*, 1993;Le Roy and Wrana, 2005). SVE occurs when nerve terminals retrieve empty synaptic vesicles after stimulated exocytosis to enable refilling of these vesicles with neurotransmitters for a new round of exocytosis. It is mediated by dynamin I. SVE and RME utilize distinct isoforms of the same proteins and have other mechanistic distinctions, for example SVE is stimulated by calcium-dependent activation of the phosphatase calcineurin (Liu and Robinson, 1995;Hinshaw, 2000). Dynamin I, II and III are all found in neurons, but dynamin I is neuronal-specific and is expressed at much higher than either of the others (Ferguson *et al.*, 2007).

Dynamin is a 96 kDa GTPase enzyme involved in membrane constriction and fission during RME and SVE. At a late stage of the process dynamin assembles into rings to form a collar or helix around the neck of the invaginating vesicles. Upon GTP hydrolysis the vesicle is pinched from the plasma membrane (McNiven, 1998) by a conformational twist in the

Molecular Pharmacology Fast Forward. Published on August 16, 2007 as DOI: 10.1124/mol.107.034207
This article has not been copyedited and formatted. The final version may differ from this version.

dynamin helix (Roux *et al.*, 2006). Dynamin is also needed for many, but not all, forms of clathrin-independent endocytosis such as phagocytosis, caveolae internalization and endocytosis of cytokine receptors in non-neuronal cells, and fast/rapid endocytosis in neurons and neuroendocrine cells (Jockusch *et al.*, 2005;Artalejo *et al.*, 1997;Hinshaw, 2000). Knockout of the dynamin I gene in mice reveals its central role in SVE, but also reveals the occurrence of dynamin I-independent SVE at the synapse, presumably mediated by dynamin II or III (Ferguson *et al.*, 2007). Dynamin contains four functional domains: an N-terminal GTPase domain, a pleckstrin homology (PH) domain, a proline-rich domain (PRD), and an assembly domain also known as GTPase effector domain (GED) (Cousin and Robinson, 2001). Overexpression of GTPase-defective dynamin mutants inhibits both RME and SVE in a variety of cells (Marks *et al.*, 2001). The PH domain of dynamin is relatively non-selective, but has a small preference for binding phosphatidylinositol-4,5-bisphosphate (PtdIns(4,5)P_2) (Salim *et al.*, 1996) which enhances its GTPase activity (Lin *et al.*, 1997;Barylko *et al.*, 1998;Vallis *et al.*, 1999) and induces cooperative dynamin helix assembly (Stowell *et al.*, 1999). Deletion of the PH domain elevates the level of dynamin's non-stimulated GTPase activity (Scaife *et al.*, 1998). Therefore each of dynamins' functional domains is an attractive target for development of dynamin inhibitors, as potential endocytosis inhibitors.

Our aim was to develop dynamin inhibitors as new tools for cell biology and also as potentially clinically useful endocytosis inhibitors. Multiple low potency and low specificity endocytosis inhibitors exist: chlorpromazine (Atwood, 2001;Wang *et al.*, 1993), concanavalin A, phenylarsine oxide (Gray *et al.*, 2001), dansylcadaverine (Davies *et al.*, 1984), intracellular potassium depletion (Larkin *et al.*, 1983), intracellular acidification (Lindgren *et al.*, 1997) and decreasing the temperature to 4°C (Wang *et al.*, 1993). Each has poor specificity and low

utility but nonetheless has contributed significantly to our understanding of endocytosis. We previously reported on the development of long chain ammonium salts (Hill *et al.*, 2004) and dimeric tyrphostins (Hill *et al.*, 2005) as the first two series of small molecule inhibitors of dynamin's GTPase activity.

Two of the most potent inhibitors from the long chain ammonium salt series of compounds were myristyl trimethyl ammonium bromide (MiTMAB, also known as tetradecyl trimethylammonium bromide or TTAB: CAS number 1119-97-7) and octadecyltrimethyl ammonium bromide (OcTMAB: CAS number 1120-02-1). Many pharmacologically active compounds are amphiphilic or hydrophobic molecules whose site of action in an organism is frequently the plasma membrane (Schreier *et al.*, 2000). They tend to self-associate and to interact with biological membranes. Amphiphilic compounds have a long hydrophobic portion and either an ionic (anionic, cationic or zwitterionic) or a non-ionic polar head group. Classes of amphiphilic drugs include phenothiazines, benzodiazepine tranquilizers, analgesics, tricyclic antidepressants and local anaesthetics (Schreier *et al.*, 2000). Trimethyl alkylammonium compounds like the MiTMAB series have pharmaceutical properties since they produce long lasting anaesthetic activity that increases with increasing alkyl chain length (Scurlock and Curtis, 1981). In the present study we report that the mechanism of dynamin inhibition by the MiTMAB series involves a surface-activity of the compounds on membranes and we show that the compounds reversibly inhibit different forms of endocytosis in multiple cell systems.

MATERIALS AND METHODS

Materials - Phosphatidylserine (PS), phenylmethylsulfonylfluoride (PMSF) and Tween 80

were from Sigma-Adrich (St Louis, CA). GTP was from either Sigma or Roche Applied Science (Germany), leupeptin was from Bachem (Bubendorf, Switzerland). Gel electrophoresis reagents, equipment and protein molecular weight markers were from Bio-Rad (Hercules, CA). Collagenase was from Roche. Paraformaldehyde (PFA) was from Merck Pty Ltd (Kilsyth, Australia). Coverslips were from Lomb Scientific (Sydney, Australia). Penicillin/streptomycin, phosphate buffered salts, foetal calf serum (FCS) and Dulbecco's Minimal Essential Medium (DMEM) were from Invitrogen (Mount Waverley, Victoria, Australia). Texas-red conjugated transferrin (Tf-TxR), Texas-red conjugated EGF (EGF-TxR) Alexa-488 conjugated EGF (EGF-A488), Alexa-594 conjugated Tf (Tf-A594), biotinylated-Tf, DAPI, FM2-10, and Fluo3-AM were from Molecular Probes (Oregon, USA). Unconjugated EGF was from Sigma-Aldrich. All other reagents were of analytical reagent grade or better.

Drugs - Drugs were from Sigma-Aldrich. The drugs were made up as stock solutions in 10-100% DMSO and diluted in 10% v/v DMSO/20 mM Tris/HCl pH 7.4 prior to use in the assay. The final DMSO concentration in the GTPase or endocytosis assays was at most 1%. The GTPase assay for dynamin I was unaffected by DMSO up to 1%. MiTMAB was dissolved as 30 mM stocks in 100% DMSO and was colourless. Stocks were stored at -20°C for several months. It was diluted into solutions of 10% DMSO (range 1-10%) made up in 20 mM Tris/HCl pH 7.4, and then diluted again into the final assay.

Protein production - Dynamin I was purified from sheep brain by extraction from the peripheral membrane fraction of whole brain (Robinson *et al.*, 1993) and affinity purification on GST-Amph2-SH3-sepharose as described (Marks and McMahon, 1998;Quan and

Molecular Pharmacology Fast Forward. Published on August 16, 2007 as DOI: 10.1124/mol.107.034207
This article has not been copyedited and formatted. The final version may differ from this version.

Robinson, 2005), yielding 8 - 10 mg protein from 250 g sheep brain. Recombinant dynamin I lacking the PH domain (dynamin I ΔPH, provided by Robin Scaife, Perth, Australia) was expressed in insect cells using baculoviral infection and was also affinity purified on GST-Amph2-SH3 sepharose beads (Salim *et al.*, 1996).

Malachite Green GTPase assay - The Malachite Green method was used for the sensitive colorimetric detection of orthophosphate (P_i). It is based on formation of a phosphomolybdate complex at low pH with basic dyes, causing a colour change (Hohenwallner and Wimmer, 1973;Van Veldhoven and Mannaerts, 1987;Geladopoulos *et al.*, 1991). The assay procedure has previously been described in detail and is based on stimulation of native sheep brain-purified dynamin I by sonicated phosphatidylserine (PS) liposomes (Quan and Robinson, 2005). However, in our earlier studies we used 200 nM dynamin I (Hill *et al.*, 2005;Hill *et al.*, 2004;Quan and Robinson, 2005) while in the present study we used 20 nM. This slightly reduced the IC_{50} values for MiTMAB analogues we previously reported (Hill *et al.*, 2004). In brief, purified dynamin I (20 nM) (diluted in dynamin diluting buffer: 6 mM Tris/HCl, 20 mM NaCl, 0.02% Tween 80, pH 7.5) was incubated in GTPase buffer (10 mM Tris/HCl, 10 mM NaCl, 2 mM Mg^{2+}, 0.05% Tween 80, pH 7.5, 1 μg/mL leupeptin and 0.1 mM PMSF) and GTP 0.3 mM in the presence of test compound for 30 min at 37ºC. The final assay volume was 150 μL. The assay was conducted in round bottomed 96 well plates. The incubations of the plate were performed in a dry heating block with shaking at 300 rpm (Eppendorf Thermomixer). Dynamin activity was measured as phospholipid stimulated with addition of different concentrations of phosphatidylserine liposomes. The reaction was terminated with 10 μL of 0.5 M EDTA pH 8.0 and the samples were stable for several hours at room temperature. To each well added

40 μL of Malachite Green solution (2% w/v ammonium molybdate tetrahydrate, 0.15% w/v malachite green and 4 M HCl: the solution was passed through 0.45 μm filters and stored in the dark for up to 2 months at room temperature). Colour was allowed to develop for 5 min (and was stable up to 2 h), and the absorbance of samples in each plate was determined on a microplate spectrophotometer at 650 nm. Phosphate release was quantified by comparison with a standard curve of sodium dihydrogen orthophosphate monohydrate (baked dry at 110°C overnight) which was run in each experiment. GraphPad Prism 4 (GraphPad Software Inc., San Diego, CA) was used for plotting data points and analysis of enzyme kinetics using non-linear regression. The curves were generated using the Michaelis-Menten equation $v = V_{max}[S]/(K_m+[S])$ where S = PS activator or GTP substrate. After the V_{max} and K_m values were determined, the data was transformed using the Lineweaver-Burke equation $1/v=1/V_{max} + (K_m/V_{max})*(1/[S])$.

Phospholipid binding - Dynamin I (520 nM) purified from whole sheep brain was incubated with PS liposomes (100 μM, sonicated into 30 mM Tris/HCl pH 7.4) in 100 μl of assembly buffer (1 mM EGTA, 30 mM Tris, 100 mM NaCl, 1 mM DTT, 1 mM PMSF, and a Complete protease inhibitor cocktail tablet per 50 ml (Roche)) for 30 min at room temperature (22°C). The samples were centrifuged at 14,000 g for 15 min to separate lipid-bound (P) and free (S) dynamin and the fractions analysed by gel electrophoresis on a 12% SDS polyacrylamide gel followed by staining with Coomassie Brilliant Blue.

Texas red-Tf and Alexa 488-EGF uptake - COS-7, HeLa and A431 cells were cultured in DMEM supplemented with 10% FCS at 37°C in 5% CO_2 in a humidified incubator. Tf and EGF uptake were analysed based on methods previously described (van der Bliek *et al.*,

1993). Briefly, cells were plated on glass coverslips (coated with superfibronectin for A431 cells or poly-D-lysine for COS-7 and HeLa cells) to 60% confluency. The cells were serum-starved overnight (16 h) in DMEM minus FCS. Cells were then incubated with MiTMAB (usually 30 μM) or vehicle for 10 or 15 min prior to addition of 5 μg/ml Tf-TxR or 1 μg/ml EGF-A488 for 15 min at 37°C. For washout experiments, this involved one complete change of media (-FCS) after drug treatment and incubation at 37°C for 30 min, after which 600 ng/ml EGF-TxR and 5 μg/ml of Tf-A594 was added to each well and incubated for 10 min at 37°C. Cell surface-bound Tf or EGF was removed by incubating the cells in an ice cold acid wash solution (0.2 M acetic acid + 0.5 M NaCl, pH 2.8) for 15 min. Cells were immediately fixed with 4% PFA for 10 min then washed 3 times with PBS. Nuclei were stained using DAPI. Coverslips were mounted using mounting medium containing DABCO and the fluorescence was monitored using a Leica DMLB bright field microscope and SPOT digital camera.

Quantitative analysis of the inhibition of EGF endocytosis in COS-7 cells was performed on large numbers of cells by an automated process. COS-7 cells were grown in poly-D-lysine-coated 96 well plates and pre-incubated with varying concentrations of drugs for 15 min prior to addition of 1 μg/ml EGF-A488 for 10 min at 37°C. All conditions were carried out in triplicate. Cells were washed twice with ice cold PBS and subjected to an acid wash (0.2 M acetic acid, 0.5 M NaCl, pH 2.8) at 4°C for 10 min to remove surface bound EGF. Cells were washed again with PBS before fixation in 4% PFA (pH 7.4). Nuclei were stained with DAPI. Green (EGF-A488) and blue (DAPI) images were collected automatically using an Olympus IX81 epifluorescence microscope. Nine images were collected from each well, averaging 40-50 cells per image. The average integrated intensity of EGF-A488 signal per cell was

calculated for each well using Metamorph (Molecular Devices, Sunnyvale, CA), and the data expressed as a percentage of control cells (vehicle treated). The average number of cells for each data point was ~1,200. IC_{50} values were calculated using GraphPad Prism 4 (GraphPad Software Inc.) and data was expressed as mean ± 95% confidence interval (CI) for 3 wells and ~1,200 cells.

Tf and EGF binding assays - For the Tf binding assay, 1.5 x 10^5 COS-7 cells were cultured in 6-well culture plates for 2 days then the cells were serum starved for 2 h in DMEM minus FCS. Cells were then incubated with MiTMAB (30 μM) or DMSO (vehicle control) for 10 min at 37°C then placed on ice. Biotinylated-Tf (10 μg/ml) was then added to cells for the indicated times and then washed 4 times with ice cold PBS. Cells were lysed for 10 min with Lysis buffer (20 mM Tris/HCl pH 7.4, 2 mM EDTA, 2 mM EGTA, 1% TritonX-100, 10 μg/ml leupeptin, 1 mM PMSF, Complete protease inhibitor tablet (Roche), 2 mM imidazole, 1 mM sodium fluoride, 2 mM sodium orthovanadate, 1 mM sodium molybdate, 4 mM sodium tartrate dihydrate), centrifuged at 14,000 g for 10 min and supernatant was harvested as the total cell lysate. Lysates for each condition were resolved on a 10 % SDS-polyacrylamide gel and transferred onto Protran immobilized nitrocellulose membrane (PerkinElmer Life Sciences, Boston, MA). The membranes were probed with avidin conjugated HRP (Molecular Probes) and signal was developed with SuperSignal West Pico chemiluminescence (Pierce Chemical, Rockford, IL). Intensity of the biotinylated-Tf was normalized against an endogenous biotinylated COS-7 cell protein on the same blots and the range of values (n=2) was plotted.

For the EGF binding assay and microscopy image analysis, A431 cells were grown overnight

on 22 mm coverslips coated with 1 ml of 5 μg/ml superfibronectin (Sigma-Aldrich). Cells were serum starved for 2 h and then treated with either DMSO (vehicle control) or 30 μM MTMAB for 10 min at 37°C. Cells were then placed on ice and incubated with EGF-A488 (600 ng/ml) for 30 min, fixed in 4% paraformaldehyde (pH 7.5) at RT and counterstained with DAPI. Images were collected using Metamorph acquisition software (Molecular Devices, Sunnyvale, CA)), an Olympus IX81 Motorised Inverted Microscope, a Hamamatsu ORCA-ERG (Hamamatsu Photonics, Japan) 12 bit FireWire Cooled CCD Camera and a UPLAPO100XOI3 objective. Z stacks were collected at 0.2 um intervals (~70 images/stack) and 3D deconvoluted using AutoDeblur (AutoQuant Imaging, Inc., Troy, NY). A maximum projection image was then generated. Images are representative of 2 independent experiments.

EGFR activation and Western blot analysis - A431 cells were cultured in 100 mm dishes to 80% confluency then the cells were serum starved overnight (16 h) in DMEM minus FCS. Cells were then incubated with MiTMAB (30 μM), DMSO (vehicle control) or Genistein (30 μM; negative control) for 10 min prior to addition of unconjugated EGF (100 ng/ml) for 10 min at 37°C. All conditions were carried out in duplicate. After 10 min incubation, cells were placed on ice and washed 4 times with ice cold PBS. Total cell lysates were prepared by incubating cells for 10 min with Lysis buffer. The mixture was then centrifuged at 14,000 g for 10 min and supernatant was harvested as the total cell lysate. Fifty μg of total cell lysate for each condition was resolved on a 12 % SDS-polyacrylamide gel and then transferred onto Protran immobilized nitrocellulose membrane (PerkinElmer). The membranes were probed with PY20 phosphotyrosine mouse monoclonal antibody (BD Biosciences, San Jose, CA). The secondary antibody was goat anti-mouse polyclonal antibody conjugated to HRP (Dako,

Denmark) and signal was developed with SuperSignal West Pico chemiluminescence (Pierce Chemical). The membranes were then stripped with 0.2 M NaOH and reprobed for endogenous EGFR using EGFR 1F4 mouse monoclonal antibody (Cell Signaling Technology, Danvers, MA) and developed as above. Western blots were scanned using the BioRad GS800 Densitometer (BioRad, Hercules, CA) and densitometry analysis was performed by Quantity One software (BioRad). EGFR phosphotyrosine (pEGFR) signal was normalized against total EGFR signal and expressed as relative intensity (%) of the stimulated control (DMSO) condition and the average of range of values (n=2) was plotted.

PH domain localization in cells - The cDNA of the PH domain of dynamin 1 (rat sequence, amino acids Thr-511 to Lys-635) was cloned by PCR and recombination into the GATEWAY entry vector pDONR201 (Invitrogen). The cDNA was subcloned by recombination into pcDNA-DEST53 (mammalian N-terminal GFP-tag) expression vector (Invitrogen). HeLa or COS-7 cells were plated on glass coverslips and transfected with 0.2 μg of GFP-dyn 1-PH or GFP-PLCδ-PH DNA per well (24 wells/550 μl final volume/well) using FuGENE according to the manufacturer's instructions and analysed 48 h after transfection. Cells were serum-starved for 2 h at 37°C, after which they were treated with 30 μM MiTMAB or 30 μM myristic acid for 10 min, and incubated a further 20 min in the presence of Tf-A594 or EGF-TxR as an internal positive controls that the drugs worked and that the DNA construct was not inhibitory (Supplementary Figure S1). Cells were then fixed with 3% PFA in PBS. The distribution of GFP-dyn 1-PH, GFP-PLCδ-PH and Tf-A594 or EGF-TxR was determined by fluorescence microscopy in the green and red channels, respectively. Optical sections were analysed by confocal laser scanning microscopy using a Leica TCS SP2 system (Leica Microsystems, Heidelberg, Germany).

Molecular Pharmacology Fast Forward. Published on August 16, 2007 as DOI: 10.1124/mol.107.034207
This article has not been copyedited and formatted. The final version may differ from this version.

Chromaffin cells, carbon fibre amperometry and Ca $^{2+}$ imaging - Adult male Wistar rats were killed by carbon dioxide inhalation as approved by the Monash Medical Centre Animal Care Committee. Adrenal glands (4-6) were dissected in cold Ca^{2+}-free Locke's buffer consisting of: 154 mM NaCl, 5.6 mM KCl, 3.6 mM $NaHCO_3$, 5.6 mM glucose, 5.0 mM HEPES, pH 7.4 and then incubated with 3 mg/ml collagenase type A in Locke's buffer in a shaking bath at 37°C for 15, 10, and 5 min with trituration between incubations. After centrifugation at 400 g for 5 min cells were resuspended in DMEM medium supplemented with 1% penicillin/streptomycin and 10% FCS, filtered through a nylon mesh, centrifuged at 400 g for 5 min, plated on 35 mm culture dishes and incubated at 37°C with 10% CO_2. Cells were maintained in primary culture for 5-7 days prior to experiments to maximise their secretory capacity. Catecholamine release from single chromaffin cells was measured using carbon fibre amperometry as previously described (Chow *et al.*, 1992). A voltage of +800 mV was applied under voltage clamp conditions to a carbon fibre electrode (ProCFE, Dagan Corporation) on an individual chromaffin cell. The current due to catecholamine oxidation was recorded with an EPC-9 amplifier and Pulse software (HEKA Electronic), sampled at 10 kHz and low-pass filtered at 1 kHz. Secretory events were analysed (Mini Analysis, version 6.0.1, Synaptosoft) for a period of 1 min from the start of exposure to the high KCl-containing (70 mM KCl replaced an equimolar amount of NaCl) bath solution. When MiTMAB or DMSO-containing solutions were applied, secretory events were analysed for 10 min. Standard bath solution contained: 140 mM NaCl, 5 mM KCl, 2 mM $CaCl_2$, 1 mM $MgCl_2$, 5 mM D-glucose, and 10 mM Hepes at pH 7.4. Both control and high KCl solutions were applied to cells using a gravity perfusion system, the outlet of which was within 500 mm of the recorded cell. All experiments were carried out at room temperature (22-24°C). After the

first stimulation, cells were continuously washed in control bath solution for 5 min to allow them to recover then a solution containing either MiTMAB (30 μM from a stock of 10 mM in DMSO) or an equivalent volume of DMSO alone (control) was continuously applied to cells for 10 min at room temperature. Cells were stimulated a second time with high KCl solution. For single cell Ca^{2+} imaging, cells were loaded with the Ca^{2+} indicator Fluo-3 AM (5 μM) in serum-free DMEM at 37°C for 45 min. Before the recording, the cells were rinsed with, and kept for at least 10 min in bath solution to allow for full de-esterification of the dye. The cells were perfused at 2 ml/min. Confocal microscopy was applied using an argon ion laser (Olympus, Australia) scanning at a peak of 488 nm and emitted light was detected at wavelengths >515 nm. Images were captured and analysed using supplied software (Fluoview-300, Olympus). Laser intensity was reduced to 5% of maximum by use of neutral density filters and the scan rates kept at 1 scan per 5 s to avoid photobleaching. Changes in intracellular Ca^{2+} levels were taken as the ratio of the maximum mean pixel value of the whole cell during stimulation compared to that in the control period in order to rule out the influence of cell batch or Fluo-3 loading efficiencies (Keating *et al.*, 2001). This ratio is calculated according to the equation: $R = (F-F_{min}) / F_{min}$, (where R = ratio of fluorescence change, F_{min} = mean fluorescence intensity during control period, and F = maximum fluorescence intensity during stimulation). All results were normalised to the response to high KCl under control conditions, which was assigned a value of 1. All data are displayed as mean ± SEM and data were tested for significant differences using one-way ANOVA for comparisons between groups and Student's paired t-test for comparisons within groups. $p<0.05$ was set as the limit for statistical significance.

Endocytosis and exocytosis in synaptosomes - Both assays were performed in rat brain percoll

purified synaptosomes (Dunkley *et al.*, 1986) as previously described using FM2-10 uptake to measure endocytosis (Cousin and Robinson, 1998;Cousin and Robinson, 2000) or enzyme-linked fluorescent detection of released glutamate (Nicholls and Sihra, 1986;Cousin and Robinson, 2000). Synaptosomes were incubated with either plus (118.5 mM NaCl, 4.7 mM KCl, 1.18 mM $MgCl_2$, 1.3 mM $CaCl_2$, 0.1 mM K_2HPO_4, 20 mM Hepes, 10 mM glucose, pH 7.4) or minus (1 mM EGTA, no $CaCl_2$) Krebs-like medium supplemented with 30 μM MiTMAB for 10 min prior to stimulation with 30 mM KCl where indicated.

Electron microscopy - Purified synaptosomes were incubated for 5 min in Krebs-like medium containing 1.2 mM Ca^{2+} then stimulated with 41 mM KCl for 2 min at 37°C. Synaptosomes were either untreated or preincubated with 30 μM MiTMAB 5 min prior to KCl addition. After stimulation synaptosomes were pelleted in a microfuge at 14,000 g for 2 min at room temperature then fixed by gentle resuspension in Krebs-like medium supplemented with 5% glutaraldehyde for 1 h at 4°C. Synaptosome pellets were gently washed 3 times with Krebs buffer with low spins (2,350 g) for 7 min then gently resuspended in a 10% BSA in H_2O for 20 min at room temperature. The synaptosomes were then re-centrifuged at low speed, overlaid with fixative (1% glutaraldehyde in Krebs-like medium) and incubated at 4°C overnight. The pellets were rinsed, stained in a buffered solution of osmium tetroxide for 3 h, rinsed and incubated for 1 h in 2% aqueous uranyl acetate. Samples were dried by a series of sequential 10 min washes: 50% ethanol and 0.1% NaCl, 70% ethanol and 0.1% NaCl, 95% ethanol and 0.1% NaCl, 100% ethanol and 0.1% NaCl twice and 100 % acetone twice. The synaptosomes were infiltrated with an acetone/resin mixture (1:1) for 1 h, washed 3 times for 10 min in Spur's epoxy resin at 70°C, then embedded within conical shaped moulds filled with Spur's epoxy resin for 10 h at 70°C. An ultramicrotome Ultracut-E (Reichert, Germany)

was used to obtain 0.08 μm epoxy sections from the resin blocks. The sections were cut with a diamond knife (Diatome, Switzerland), floated on water drops, placed on electron microscopy grids and double stained: first using 2% uranyl acetate in ethanol for 15 min and then Reynold's lead citrate for 4 min. The grids were washed in water, touch dried using absorbent filter paper and stored until analysis with an electron microscope. Analysis was performed on a Philips 1L-BioTwin electron microscope (Eindhoven, The Netherlands) and pictures were printed on electron microscope plate film (Kodak, 4489, 8.3 cm X 10.2 cm).

RESULTS

MiTMAB inhibits the GTPase activity of dynamin I

Myristyl trimethyl ammonium bromide (MiTMAB) is a 14 carbon alkyl chain with a trimethylated ammonium head group and a bromide counter ion (Table 1, entry 5) previously reported to inhibit dynamin I GTPase activity (IC_{50} 5.79 ± 2.06 μM) (Hill *et al.*, 2004). In the present study the GTPase assay was redesigned to utilize lower dynamin concentrations (20 nM instead of 200 nM) and the activity of a number of other long chain amines and ammonium salts (MiTMAB analogues) were reassessed (Table 1). The new IC_{50} for MiTMAB was little changed (3.1 ± 0.2 μM, Table 1). The full concentration response curve is shown in Fig 1A. When the alkyl chain length was increased to 18 carbons (octadecyl trimethyl ammonium bromide (OcTMAB)) the potency increased to 1.9 ± 0.2 μM, and when the chain length was decreased to the dodecyl form potency dropped to 9.0 ± 1.4 μM (Table 1). The simpler fatty amine salt analogues of these cationic amphiphiles were also examined. Replacing the trimethyl bromide head with an amine or dimethyl amino group produced IC_{50}'s of 6.5 ± 1.0 μM and 9.2 ± 0.96 μM (respectively, Table 1). The acid form of MiTMAB, myristic acid, was inactive. Therefore a diverse range of cationic amphiphiles exhibits a tight

structure-activity relationship towards dynamin I.

MiTMAB targets the dynamin I-phospholipid interaction

Phosphatidylserine (PS) or PtdIns(4,5)P_2 binds the PH domain of dynamin, enhances its GTPase activity (Zheng *et al.*, 1996;Lin *et al.*, 1997) and induces cooperative helix assembly (Stowell *et al.*, 1999). The dynamin I GTPase assay employed here utilizes phosphatidylserine (PS) liposomes to maximally activate dynamin I. The MiTMAB series of compounds are surface-active and predicted to alter protein-lipid interactions (Scurlock and Curtis, 1981;Schreier *et al.*, 2000). At high concentrations (at, or exceeding, the critical micellar concentration (cmc, see discussion)) these compounds are cationic surfactants, as observed for other pharmacologically active cationic amphiphilic compounds like chlorpromazine or imipramine (Ahyayauch *et al.*, 2002). Therefore, several approaches were used to determine whether MiTMAB targets the dynamin-phospholipid interaction. Firstly, the effect of MiTMAB on the GTPase activity of full-length wild type (WT) dynamin I purified from sheep brain was compared with that of a recombinant dynamin I lacking the PH domain, dynamin I-ΔPH (Scaife *et al.*, 1998). WT dynamin I GTPase activity was stimulated by PS liposomes (1.2 μM) and was inhibited by MiTMAB (10 and 30 μM) (Figure 1B). In contrast, dynamin I-ΔPH was constitutively active and its activity was unaffected by further PS addition (Figure 1C), as previously reported (Scaife *et al.*, 1998;Vallis *et al.*, 1999). The GTPase activity of dynamin I-ΔPH was insensitive to MiTMAB (10 or 30 μM, Figure 1C). This reveals that MiTMAB inhibits the liposome stimulated dynamin I GTPase activity by targeting the dynamin-phospholipid interaction.

The second approach examined dynamin I binding to liposomes using a sedimentation assay.

Molecular Pharmacology Fast Forward. Published on August 16, 2007 as DOI: 10.1124/mol.107.034207
This article has not been copyedited and formatted. The final version may differ from this version.

In this assay dynamin and liposomes are co-incubated and the extent of their interaction is revealed by sedimentation of dynamin by centrifugation. This is a dynamin-phospholipid interaction effect, since mutations in the PH domain that block phospholipid interaction are known to arrest dynamin sedimentation (Vallis *et al.*, 1999). Dynamin alone (520 nM) did not sediment in this assay, as it remained largely in the supernatant (Figure 1D, lanes 1-2), but in the presence of liposomes (100 μM) it was found in the pellet (lanes 3-4). Phospholipid binding was unaffected by the vehicle control DMSO (lanes 5-6), however MiTMAB reduced lipid binding in a concentration-dependent manner (lanes 7-16). There was a 50% block in dynamin sedimentation at 100 μM MiTMAB. The apparent decrease in potency compared with the IC_{50} in the GTPase assay is likely due to the much higher dynamin and liposome concentrations used in this assay. In addition, MiTMAB does not affect dynamin self-assembly in a sedimentation assay (data not shown). The result suggests MiTMAB prevents dynamin association with phospholipids but not dynamin oligomerization.

The third approach was to investigate the kinetics of dynamin's GTPase activity in the presence of different concentrations of liposomes or GTP. Kinetic analysis using increasing concentrations of GTP revealed the maximal velocity of dynamin I GTPase activity, V_{max}, was 430 ± 57 nmol/mg/min and the Michaelis-Menten constant, K_m, was 20.9 ± 10 μM. In the presence of MiTMAB, the V_{max} decreased and K_m increased with increasing concentrations of the drug (data not shown). The Lineweaver-Burke plot shows non-competitive inhibition with respect to GTP (Figure 2A-B). Therefore MiTMAB does not compete with GTP for binding to dynamin's GTPase domain. Using increasing concentrations of PS, the V_{max} was 427 ± 40 nmol/mg/min, and the K_m was 3.1 ± 0.9 μM (Figure 2C-E). Lineweaver-Burke double reciprocal plots indicated competitive inhibition

Molecular Pharmacology Fast Forward. Published on August 16, 2007 as DOI: 10.1124/mol.107.034207
This article has not been copyedited and formatted. The final version may differ from this version.

with PS (Figure 2D). In the presence of MiTMAB, there was no effect on V_{max} but an increased K_m (data not shown). This indicates MiTMAB is a competitive inhibitor with respect to PS with an inhibition constant, K_i, of 940 $\pm$ 25 nM (Figure 2E). Collectively, these data show that MiTMAB is a surface-active compound that competes for PS binding to the dynamin I PH domain.

MiTMAB blocks RME in non-neuronal cells

Dynamin II is essential for RME, since dominant-negative mutations in its GTPase domain that cause defects in GTP binding or ablation of its GTPase activity result in arrest of Tf uptake in non-neuronal cells (Damke *et al.*, 2001;Koenig and Ikeda, 1989). We next determined the effect of MiTMAB on this dynamin II-dependent process in different non-neuronal cell lines. We examined the effect of MiTMAB on Tf and EGF internalization in HeLa (Figure 3), HER14, A431 and COS-7 cells (data not shown). Tf and EGF are both internalized by RME, although they traffic to different subcellular compartments after internalization (Sheff *et al.*, 2002;Gaborik and Hunyady, 2004). After 15 min of internalization under control conditions (DMSO treatment) the cells showed considerable staining of Tf-TxR (Figure 3A and 3C) in the periphery and perinuclear region of the cell, which is typical of Tf localization in early and recycling endosomes (Sheff *et al.*, 2002;Gaborik and Hunyady, 2004). The same cells showed punctate intracellular staining of EGF-A488 (Figure 3B and 3C) in the perinuclear region, typical of EGF internalization to late endosomes and lysosomes. After 10 min preincubation, MiTMAB (30 μM) reduced RME of Tf (Figure 3D) and EGF (Figure 3E), and internalization was completely blocked at 100 μM (Figure 3G and 3H). Note that cell morphology was unaffected by the drug treatment (Figure 3I), even after 30 min exposure (data not shown), indicating that there was no membrane

Molecular Pharmacology Fast Forward. Published on August 16, 2007 as DOI: 10.1124/mol.107.034207
This article has not been copyedited and formatted. The final version may differ from this version.

disruption. The results were confirmed in two other cell lines (data not shown, also see below for COS-7 cells). Therefore, MiTMAB effectively blocks RME of Tf and EGF into non-neuronal cells.

To determine whether the effects of MiTMAB are reversible we examined the recovery of RME in A431 cells after an endocytic block with MiTMAB followed by drug washout. EGF endocytosis was greatly reduced in A431 cells incubated with MiTMAB (30 μM for 10 min) (Figure 3J-K). When endocytosis was measured 30 min after washout of MiTMAB it was found to have returned to control levels (Figure 3L). The same results were obtained in these cells for RME of Tf (data not shown). Therefore, the effects of MiTMAB in cells are reversible 30 min after treatment. The same results were obtained after only a 5 min washout (data not shown), suggesting MiTMAB is a rapidly reversible inhibitor.

To quantify the effect of MiTMAB in COS-7 cells we established an automated quantitative RME assay based on endocytosis of EGF-A488. The IC_{50} for inhibition of RME by MiTMAB in COS-7 cells was 20.9 ± 3.2 μM (Figure 3M), which compares favourably with the IC_{50} for dynamin inhibition *in vitro*. OcTMAB was slightly more potent, DoTMAB was 8-fold less potent, and tetradecylamine was 2-fold less potent (Figure 3M-3P). 2-(dimethylamino) ethyl myristate and myristic acid were both without effect. This rank order of potency for RME inhibition closely matches the rank order of potency for inhibition of dynamin's GTPase activity (Table 1), suggesting that the mechanism of inhibition is via dynamin. As expected, the ester derivative of myristic acid, 2-(dimethylamino) ethyl myristate, had almost no cellular activity despite good *in vitro* potency. This compound was designed as a pro-drug to be rapidly cleaved to myristic acid (which is inactive) and

Molecular Pharmacology Fast Forward. Published on August 16, 2007 as DOI: 10.1124/mol.107.034207
This article has not been copyedited and formatted. The final version may differ from this version.

dimethylamino ethanol by endogenous intracellular esterases.

MiTMAB does not block Tf or EGF binding nor EGFR activation

To determine that the effect of MiTMAB on RME is intracellular and not due to blocking initial ligand binding to its receptor we examined its effect on Tf and EGF binding to their respective cell surface receptors. It is well known that these ligands bind to their receptors on the cell surface in ice cold conditions and do not get internalized. Therefore we examined the effect of MiTMAB on cell surface binding of biotinylated-Tf (10 μg/ml) to COS-7 cells in ice cold conditions and measured the amount of Tf binding using Western blot analysis and densitometry. Tf binding was detected at relatively high levels 1 min after addition of Tf in both control (vehicle only) and MiTMAB (30 μM) treated cells (Figure 4A). Tf binding was maximal within 5 min and maximal binding was not altered in MiTMAB treated cells. Therefore, MiTMAB does not interfere with Tf binding to cell surface receptors.

To search for potential effects of MiTMAB on EGF binding to the EGFR we used deconvolution fluorescence microscopy to detect total surface binding in Z stack images. Due to the low levels of EGFR in many cell types and difficulties to isolate detectable levels of the EGFR in cell lysates, we used A431 human carcinoma cells because they overexpress the endogenous EGFR due to genomic amplification. In vehicle treated control cells EGF-A488 bound to the cell surface and was not internalized at 4°C (Figure 4B-C and Supplementary Movie S1). In cells treated with MiTMAB (30 μM for 10 min) EGF-A488 the total amount of binding to the cell surface was unchanged. However distribution of the cell surface binding was altered by MiTMAB treatment, resulting in increased localization of the EGFR at cell-cell contacts (Figure 4D-E and Supplementary Movie S2). MiTMAB was also without

effect on total cellular expression levels of the EGFR (Figure 4F). Together, this suggests that MiTMAB produces moderate redistribution of the EGFR, but does not alter total receptor levels.

By measuring receptor autophosphorylation on tyrosine residues we next asked whether MiTMAB inhibits EGFR activation. A431 cells stimulated with EGF (100 ng/ml) for 10 min had increased EGFR autophosphorylation (Figure 4F and 4G). Both MiTMAB and OcTMAB were without effect. In contrast, genistein (30 μM for 10 min), a known protein tyrosine kinase inhibitor that inhibits EGFR autophosphorylation, abolished EGF-stimulated autophosphorylation. Therefore, MiTMAB and OcTMAB do not appear to inhibit RME via effects on signalling from the activated EGFR.

MiTMAB blocks PH domain localization to the plasma membrane

Dynamin associates with the plasma membrane via its PH domain interaction with the membrane phospholipids. Mutations in the dynamin PH domain block RME (Achiriloaie *et al.*, 1999). To correlate the *in vitro* observations that MiTMAB blocks the dynamin-phospholipid interaction and to determine whether MiTMAB targets dynamin localization to the plasma membrane during RME, HeLa cells were transfected with a GFP-dyn I-PH construct to examine its membrane association in cells using confocal microscopy. Expression of GFP-dyn I-PH domain in control cells revealed a predominantly cytosolic distribution as expected, but a significant pool was specifically associated with the plasma membrane in all cells (Figure 4A-B). Higher magnification of the boxed regions illustrates the membrane association (Figure 4A'-B'). When cells were treated with MiTMAB (30 μM for 30 min) the staining of the plasma membrane was abolished (Figure 4C-D, boxed region,

Molecular Pharmacology Fast Forward. Published on August 16, 2007 as DOI: 10.1124/mol.107.034207
This article has not been copyedited and formatted. The final version may differ from this version.

and zoomed regions in Figure 4C'-D'). The inactive analogue myristic acid (30 μM) had no effect (Figure 4E-F, boxed region, and zoomed regions in Figure 4E'-F'). Therefore MiTMAB prevented GFP-dyn I-PH domain localization to the plasma membrane of HeLa cells, suggesting that the arrest of RME was due to blocking dynamin recruitment to the membrane. To confirm that transfection alone of the GFP-dyn I-PH domain construct did not block RME, endocytosis of Tf-A594 and EGF-TxR was monitored simultaneously in these experiments (Supplementary Figure S1). RME was unaffected by transfection alone but was almost abolished in the cells treated with MiTMAB. In contrast, cells treated with myristic acid showed normal Tf internalization (data not shown). Next we examined the effect of MiTMAB on an unrelated PH domain protein with high affinity for membrane phospholipids - PLCδ1-PH domain (Garcia *et al.*, 1995). MiTMAB also blocked its localization to the plasma membrane in HeLa cells and myristic acid was without effect (Supplementary Figure S2). This suggests that MiTMAB inhibits the PH domain-phospholipid interactions of proteins in addition to dynamin.

MiTMAB blocks KCl-induced exocytosis in rat adrenal chromaffin cells

To determine whether MiTMAB inhibits SVE we used two models for neuronal exocytosis and endocytosis. Firstly, we investigated whether MiTMAB inhibited endocytosis in adrenal chromaffin cells, a neuroendocrine cell that releases catecholamines on depolarization, which can be monitored using carbon fiber amperometry due to the charged nature of catecholamines. Since exocytosis and endocytosis are coupled in such excitable cells, it is first necessary to determine the effects on exocytosis of any potential inhibitor, prior to determining its effect on endocytosis. A block in the former will non-specifically inhibit the latter, masking any specific endocytic effect. The chromaffin cells robustly secreted

catecholamines in response to a first 70 mM KCl (S1) stimulus (Figure 5A). The same magnitude of exocytosis was reproducibly observed after a second (S2) (Figure 5A) or third (S3) stimulation (data not shown). However, when MiTMAB (30 μM) was applied for 10 min between stimuli, surprisingly, exocytosis was abolished at S2 (Figure 5B). Quantitative analysis of the number of events/min and total charge due to catecholamine release revealed the strong exocytosis inhibition (Figure 5C-D). The compound did not induce exocytosis on its own nor depolarise the cells, suggesting that the membrane potential was intact. Since KCl-induced exocytosis is dependent on Ca^{2+} entry, we explored this as a potential mechanism for the effect. Chromaffin cells were loaded with the Ca^{2+}-sensitive fluorescent dye, Fluo-3. Fluorescence increases, indicative of increased intracellular Ca^{2+} concentrations, were observed upon stimulation with 70 mM KCl for 1 min (Figure 5E). However, high KCl-induced Ca^{2+} entry was abolished after 10 min incubation with MiTMAB. This was not due to an immediate extracellular ion channel pore block by MiTMAB, as a significant amount of Ca^{2+} entry still occurred ($p<0.01$), albeit at 20% of the original value, in cells after just 1 min incubation with MiTMAB (n=10, Figure 5F). The results reveal that MiTMAB blocks exocytosis in chromaffin cells by reducing Ca^{2+} entry via an intracellular site of action, presumably Ca^{2+} channels. The data also indicate that the effect of MiTMAB on endocytosis cannot be assessed in these particular cells.

MiTMAB blocks SVE and not exocytosis in synaptosomes

The Ca^{2+} channels and other voltage-regulated ion channels in distinct cell types are different. We therefore examined the effect of MiTMAB on SVE in a population of rat brain nerve terminals (synaptosomes) using styryl-dye approaches. We first examined endogenous glutamate release and found that preincubation with MiTMAB (30 μM, 10 min) had no effect

Molecular Pharmacology Fast Forward. Published on August 16, 2007 as DOI: 10.1124/mol.107.034207
This article has not been copyedited and formatted. The final version may differ from this version.

on KCl-evoked Ca^{2+}-dependent glutamate release and thus SV exocytosis (Figure 6A). SVE was monitored using an established SV turnover assay which utilizes the activity-dependent dye FM2-10 (Cousin and Robinson, 2000). MiTMAB significantly reduced KCl-evoked uptake of FM2-10 compared to control (Figure 6B). Since FM2-10 uptake reflects not only on SVE but also the prior round of exocytosis, we appraised the specific effect of MiTMAB on SVE by calculating retrieval efficiency, which is a ratio of the amount of SVE divided by amount of exocytosis (Cousin and Robinson, 2000): where a value less than one indicates a selective SVE inhibition. MiTMAB significantly reduced retrieval efficiency to 0.76 ± 0.08 (Fig 6C), indicative of specific block in SVE. Therefore MiTMAB selectively blocks SVE but not exocytosis in synaptosomes.

To confirm the block in SVE in synaptosomes by an independent approach, we used an electron microscope (EM)-based method to reveal inhibition of SVE in synaptosomes (Tan *et al.*, 2003). Synaptosomes at rest or depolarized with KCl (2 min) exhibited normal morphology by EM (Figure 6D-E). Normal nerve terminals were characterised by: i) a smooth, sealed plasma membrane; ii) being mostly filled with small SVs; iii) almost always containing one or more normal mitochondrial profiles and iv) occasionally containing a synapse and associated postsynaptic density (if sectioned at the appropriate angle). We found that pretreatment with MiTMAB (30 μM) had no effect on nerve terminal morphology in resting (unstimulated) synaptosomes (Figure 6F). However, when the synaptosomes were depolarized with 30 mM KCl for 2 min after MiTMAB pretreatment, there was a massive depletion of SVs, consistent with a specific SVE block (Figure 6G-I). This confirms that MiTMAB inhibits dynamin I-dependent SVE in synaptosomes.

Molecular Pharmacology Fast Forward. Published on August 16, 2007 as DOI: 10.1124/mol.107.034207
This article has not been copyedited and formatted. The final version may differ from this version.

DISCUSSION

The large GTPases dynamin I and II are essential for many forms of membrane internalization in eukaryotic cells (Hinshaw, 2000). Therefore small molecule inhibitors with different mechanisms of action on these key enzymes should prove to be important tools for greater understanding of their function during normal and abnormal processes. We previously reported on a series of long chain ammonium salts, such as MiTMAB and OcTMAB, as the first small molecule dynamin inhibitors (Hill *et al.*, 2004). We have now extended this observation to demonstrate that MiTMAB is a surface-active compound that targets the dynamin-phospholipid association and is a potent inhibitor of at least two forms of endocytosis in cells - RME and SVE. The compounds act rapidly to inhibit endocytosis in cells and their effects are rapidly reversed after short washout. The K_i for MiTMAB was in the high nanomolar range, indicating that it has relatively high intrinsic affinity for dynamin. The activity of these compounds partly correlated with alkyl chain length and was dependent on an amine or ammonium salt head group rather than an acid. The results provide a range of compounds with distinct potencies allowing a correlation between their *in vitro* and *in vivo* actions.

Dynamin's interaction with phospholipids is mediated by its PH domain. PH domains of proteins are known to bind acidic phospholipids, especially phosphatidylserine and specific phosphoinositides (Zheng *et al.*, 1996;Lemmon, 2003) and dynamin's PH domain has highest affinity for PtdIns(4,5)P_2 (Salim *et al.*, 1996;Barylko *et al.*, 1998). Lipid binding promotes dynamin oligomerization, which stimulates its GTPase activity (Klein *et al.*, 1998). Using three independent approaches, we attribute MiTMAB's mechanism of action is to inhibit the dynamin-phospholipid interaction. Firstly, MiTMAB was without effect on the elevated non-

stimulated GTPase activity of dynamin I-ΔPH. Secondly, MiTMAB blocked dynamin binding to phospholipid *in vitro*. Finally, enzyme kinetics showed that MiTMAB is a competitive inhibitor with PS and non-competitive with GTP. The three observations establish that MiTMAB directly interferes with PH domain binding to the phospholipid, as may have been expected for surface active cationic amphiphilic compounds. These *in vitro* observations were correlated in cells by expression of the dynamin I-PH domain. The binding of this domain to the cell membrane was abolished by MiTMAB, but not by the inactive myristic acid.

In non-neuronal cells, we found that MiTMAB inhibits Tf and EGF internalization in a variety of cell lines, suggesting a wide utility for such inhibitors as broad spectrum endocytosis inhibitors. RME is known to be dependent on the interaction of the PH domain of dynamin II with membrane phospholipids (Vallis *et al.*, 1999;Lee *et al.*, 1999) suggesting this association is the target for MiTMAB. Two further lines of evidence suggested the RME inhibition in cells occurred via inhibition of the dynamin-phospholipid interaction. Firstly, the rank order of potency of 5 of the 6 analogues on RME precisely correlated with the order of their IC_{50}'s for dynamin inhibition. Secondly, MiTMAB blocked membrane binding by the dynamin I PH domain in HeLa cells, driving it to the cytosol where it cannot support endocytosis. Thus we propose that the MiTMAB series of compounds arrest RME by interfering with the dynamin-phospholipid interaction. In contrast to the other compounds, 2-(dimethylamino) ethyl myristate was effective *in vitro,* but did not have any *in vivo* activity. It was designed as a pro-drug for intracellular delivery of myristic acid. The compound is expected to be fully membrane permeable, but presumably was rapidly cleaved to myristic acid (which is inactive) and dimethyl amino ethanol by endogenous intracellular esterases, in

a manner similar to other pro-drug esters such as FURA2-AM or BAPTA-AM. This compound will therefore be useful as a negative control in future cellular studies.

Another well-characterized endocytic route is SVE, in which dynamin I's role has been well established (Tan *et al.*, 2003;Anggono *et al.*, 2006). In these systems, exocytosis and endocytosis are highly regulated and coupled, thus blocking one route interferes with the other (Anggono *et al.*, 2006). We therefore examined exocytosis in two systems, chromaffin cells and rat brain nerve terminals (synaptosomes). Surprisingly, MiTMAB blocked exocytosis in chromaffin cells by preventing Ca^{2+} influx, hence its effect on endocytosis could not be further evaluated. Despite this, the results indicate that the compound does not cause membrane damage to the cells since basal capacitance and low intracellular Ca^{2+} concentrations were maintained in the presence of the drug. These are both independent indices of an intact plasma membrane. However, exocytosis of glutamate from synaptosomes was unaffected. This further indicates that the drug does not disrupt membrane structure since normal membrane potential was maintained in the presence of the drug. MiTMAB inhibited synaptosomal SVE by two independent criteria: styryl dye uptake and it produced morphological depletion of synaptic vesicles. Overall, our data indicate that MiTMAB inhibits two mechanistically distinct forms of endocytosis via inhibition of dynamin I or dynamin II GTPase activity. The further potential for MiTMAB to block endocytosis in animals was recently demonstrated (Hilliard *et al.*, 2006). Perfusion of exteriorised kidney with MiTMAB increased excretion of intact albumin. This suggests that MiTMAB blocks albumin endocytosis in an organ still attached to a living animal. This illustrates the potential application of an RME inhibitor like MiTMAB to studies investigating a previously unknown involvement of RME in cellular pathways.

The long chain amines and ammonium salts reported here are amphiphilic compounds with either a non-ionic (2-(dimethylamino) ethyl myristate, tetradecylamine) or a cationic polar (DoTMAB, MiTMAB, OcTMAB) head group and a hydrophobic tail. There are many drugs of clinical importance that have non-ionic or cationic amphiphilic properties (Fischer *et al.*, 1998;Ahyayauch *et al.*, 2002;Schreier *et al.*, 2000). Studies into the molecular mechanisms of pharmacological effects exerted by drugs of such structure commonly reveal they have surface-active properties such as self aggregation and the ability to interact with membranes. These properties are characterized by physicochemical parameters such as the critical micellar concentration (cmc), aggregation number and particle size (Schreier *et al.*, 2000). Self aggregation in aqueous medium and surface absorption kinetics on an artificial silica-aqueous interface have been previously studied for the MiTMAB series (Atkin *et al.*, 2003). The cmc's for DoTMAB, MiTMAB and OcTMAB are 6.3 mM, 1 mM and 0.2 mM respectively (in aqueous medium containing 10 mM potassium bromide), indicating that cmc decreases as the chain length of the hydrophobic tail increases (Atkin *et al.*, 2003). At high concentrations above its cmc MiTMAB forms mixed micelles and aggregates. The correlation between the cmc of a compound and the formation of micelle aggregates is significant to the understanding of potential membrane lipid effects of the drug, because disruption of lipid bilayer membranes may be modulated by micelle-like aggregates (Schreier *et al.*, 2000). At high concentrations above the cmc all other cationic amphiphilic compounds such as chlorpromazine and imipramine exhibit membrane solubilizing effects that are distinct from their medicinal or biological effects by 1-3 orders of magnitude (Ahyayauch *et al.*, 2002). Many lines of evidence suggest that the *in vitro* and *in vivo* inhibitory effects of MiTMAB are not a result of the compound acting like a classical detergent, solubilizing phospholipids, and

disrupting cell membranes. Firstly, the IC_{50} for dynamin inhibition is over 300-fold below the cmc. Secondly, the two sets of non-ionic and cationic head groups provide these compounds with completely different surface-active and binding properties, yet both sets are effective dynamin and endocytosis inhibitors within a narrow potency range. Thirdly, in the synaptosomal SVE assay, Ca^{2+}-dependent glutamate release was not blocked by MiTMAB, indicating a preserved membrane potential, produced by Na^+, K^+ and Ca^{2+} gradients. Electron micrographs show that the membranes of the synaptosomes remained intact and undamaged, indicating MiTMAB did not exhibit any membrane-solubilizing properties at such low concentrations. Fourthly, MiTMAB induced no cell or membrane damage to COS-7, HeLa, A431 or the excitable chromaffin cells, again suggesting the cells were otherwise viable. Finally, the effects of the drugs on endocytosis were rapidly and fully reversible. Since RME is capable of starting again this indicates the presence of relatively healthy cells.

There are potential non-specific actions of all drugs that must be considered in their application to living tissues. MiTMAB blocked Ca^{2+} influx into chromaffin cells, but not synaptosomes. The target was intra-membrane and intracellular. The block could be a voltage-gated ion channel such as the Ca^{2+} channel, since KCl depolarizes membranes and activates such channels directly. Most drugs have such secondary effects and they need to be taken into consideration in experimental design. For example the potent Cdk5 inhibitor roscovitine (Tan *et al.*, 2003) also inhibits P/Q-type Ca^{2+} channels (Yan *et al.*, 2002) yet this does not diminish its broad utility in cell biology apart from its use in certain cultured neurons (Tan *et al.*, 2003). Secondly, a drug that targets the dynamin-phospholipid interaction will likely have effects on other intracellular phospholipid binding enzymes such as we found for the PH domain of PLCδ1. Thirdly, while MiTMAB did not block EGF receptor signal

transduction or extracellular ligand binding to cell surface receptors, it altered the cell surface clustering of EGF receptors. Therefore the surface-active properties of MiTMAB can produce non-specific effects on plasma membranes with different phospholipid compositions, possibly causing membrane reorganization effects in some cells. For example, anti-depressants like clomipramine and imipramine have micellar properties and membrane interaction effects which regulate the drug's side effects (Attwood *et al.*, 1995;Ahyayauch *et al.*, 2002).

In summary, we have identified and characterized a series of long chain amine salts as inhibitors of dynamin GTPase activity, which act by preventing dynamin association with phospholipid membranes. Since treatment of neuronal and non-neuronal cells with these small molecule compounds rapidly and reversibly blocks multiple forms of endocytosis (RME and SVE), they will be useful tools to probe the function of dynamin I and II, not only in endocytosis, but for its numerous intracellular functions such as phagocytosis, post-Golgi transport, podosomes, cell migration and invasion. The MiTMAB series will also be useful for understanding the potential roles of dynamin in disease states such as cancer, inflammation, and neuropsychiatric and neurodegenerative disorders. Small molecule endocytosis inhibitors such as the MiTMAB series provide significant new cell biological tools for further molecular dissection of membrane trafficking and endocytosis pathways in eukaryotic cells.

Molecular Pharmacology Fast Forward. Published on August 16, 2007 as DOI: 10.1124/mol.107.034207
This article has not been copyedited and formatted. The final version may differ from this version.

ACKNOWLEDGEMENTS

We thank Peter Rowe for encouragement and helpful comments on the manuscript and our colleagues who provided enzymes and plasmid DNA. We also thank Dr Ross Boadle and Levina Deer for valuable technical assistance with electron microscopy.

Reference List

Achiriloaie M, Barylko B and Albanesi J P (1999) Essential Role of the Dynamin Pleckstrin Homology Domain in Receptor-Mediated Endocytosis. *Mol Cell Biol* **19**: pp 1410-1415.

Ahyayauch H, Requero M A, Alonso A, Bennouna M and Goni F M (2002) Surfactant Effects of Chlorpromazine and Imipramine on Lipid Bilayers Containing Sphingomyelin and Cholesterol. *J Colloid Interface Sci* **256**: pp 284-289.

Anggono V, Smillie K J, Graham M E, Valova V A, Cousin M A and Robinson P J (2006) Syndapin I Is the Phosphorylation-Regulated Dynamin I Partner in Synaptic Vesicle Endocytosis. *Nat Neurosci* **9**: pp 752-760.

Artalejo CR, Lemmon M A, Schlessinger J and Palfrey H C (1997) Specific Role for the PH Domain of Dynamin-1 in the Regulation of Rapid Endocytosis in Adrenal Chromaffin Cells. *EMBO J* **16**: pp 1565-1574.

Atkin R, Craig V S, Wanless E J and Biggs S (2003) The Influence of Chain Length and Electrolyte on the Adsorption Kinetics of Cationic Surfactants at the Silica-Aqueous Solution Interface. *J Colloid Interface Sci* **266**: pp 236-244.

Attwood D, Mosquera V, Garcia M, Suarez M J and Sarmiento F (1995) A Comparison of the Micellar Properties of Structurally Related Antidepressant Drugs. *J Colloid Interface Sci* **175**: pp 201-062.

Atwood WJ (2001) A Combination of Low-Dose Chlorpromazine and Neutralizing Antibodies Inhibits the Spread of JC Virus (JCV) in a Tissue Culture Model: Implications for Prophylactic and Therapeutic Treatment of Progressive Multifocal Leukencephalopathy. *J Neurovirol* **7**: pp 307-310.

Barylko B, Binns D D, Lin K M, Atkinson M L, Jameson D M, Yin H L and Albanesi J P (1998) Synergistic Activation of Dynamin GTPase by Grb2 and Phosphoinositides. *J Biol Chem* **273**: pp 3791-3797.

Chow RH, von Ruden L and Neher E (1992) Delay in Vesicle Fusion Revealed by Electrochemical Monitoring of Single Secretory Events in Adrenal Chromaffin Cells. *Nature* **356**: pp 60-63.

Cousin MA and Robinson P J (1998) Ba^{2+} Does Not Support Synaptic Vesicle Retrieval in Rat Isolated Presynaptic Nerve Terminals. *Neurosci Lett* **253**: pp 1-4.

Cousin MA and Robinson P J (2000) Ca^{2+} Inhibition of Dynamin Arrests Synaptic Vesicle Recycling at the Active Zone. *J Neurosci* **20**: pp 949-957.

Cousin MA and Robinson P J (2001) The Dephosphins: Dephosphorylation by Calcineurin Triggers Synaptic Vesicle Endocytosis. *Trends Neurosci* **24**: pp 659-665.

Damke H, Binns D D, Ueda H, Schmid S L and Baba T (2001) Dynamin GTPase Domain Mutants Block Endocytic Vesicle Formation at Morphologically Distinct Stages. *Mol Biol Cell* **12**: pp 2578-2589.

Davies PJ, Cornwell M M, Johnson J D, Reggianni A, Myers M and Murtaugh M P (1984) Studies on the Effects of Dansylcadaverine and Related Compounds on Receptor-Mediated Endocytosis in Cultured Cells. *Diabetes Care* **7 Suppl 1**: pp 35-41.

Dunkley PR, Jarvie P E, Heath J W, Kidd G J and Rostas J A (1986) A Rapid Method for Isolation of Synaptosomes on Percoll Gradients. *Brain Res* **372**: pp 115-129.

Ferguson SM, Brasnjo G, Hyashi M, Wolfel M, Collesi C, Giovedi S, Raimondi A, Gong L W, Areil P, Paradise S, O'Toole E, Flavell R, Cremona O, Miesenbock G, Ryan T A and De Camilli P (2007) A Selective Activity-Dependent Requirement for Dynamin 1 in Synaptic Vesicle Endocytosis. *Science* **316**: pp 570-574.

Fischer H, Gottschlich R and Seelig A (1998) Blood-Brain Barrier Permeation: Molecular Parameters Governing Passive Diffusion. *J Membr Biol* **165**: pp 201-211.

Gaborik Z and Hunyady L (2004) Intracellular Trafficking of Hormone Receptors. *Trends Endocrinol Metab* **15**: pp 286-293.

Garcia P, Gupta R, Shah S, Morris A J, Rudge S A, Scarlata S, Petrova V, McLaughlin S and Rebecchi M J (1995) The Pleckstrin Homology Domain of Phospholipase C-Delta1 Binds With High Affinity to Phosphatidylinositol 4,5-Bisphosphate in Bilayer Membranes. *Biochemistry* **34**: pp 16228-16234.

Geladopoulos TP, Sotiroudis T G and Evangelopoulos A E (1991) A Malachite Green Colorimetric Assay for Protein Phosphatase Activity. *Anal Biochem* **192**: pp 112-116.

Gray JA, Sheffler D J, Bhatnagar A, Woods J A, Hufeisen S J, Benovic J L and Roth B L (2001) Cell-Type Specific Effects of Endocytosis Inhibitors on 5-Hydroxytryptamine2A Receptor Desensitization and Resensitization Reveal an Arrestin-, GRK2-, and GRK5-Independent Mode of Regulation in Human Embryonic Kidney 293 Cells. *Mol Pharmacol* **60**: pp 1020-1030.

Hill TA, Odell L R, Edwards J K, Graham M E, McGeachie A B, Rusak J, Quan A, Abagyan R, Scott J L, Robinson P J and McCluskey A (2005) Small Molecule Inhibitors of Dynamin I GTPase Activity: Development of Dimeric Tyrphostins. *J Med Chem* **48**: pp 7781-7788.

Hill TA, Odell L R, Quan A, Abagyan R, Ferguson G, Robinson P J and McCluskey A (2004) Long Chain Amines and Long Chain Ammonium Salts As Novel Inhibitors of Dynamin GTPase Activity. *Bioorg Med Chem Lett* **14**: pp 3275-3278.

Hilliard LM, Osicka T M, Robinson P J, Nikolic-Paterson D J and Comper W D (2006) Characterisation of the Urinary Degradation Pathway in the Isolated Perfused Rat Kidney. *J Lab Clin Med* **147**: pp 36-44.

Hinshaw JE (2000) Dynamin and Its Role in Membrane Fission. *Annu Rev Cell Dev Biol* **16**: pp 483-519.

Hohenwallner W and Wimmer E (1973) The Malachite Green Micromethod for the Determination of Inorganic Phosphate. *Clin Chim Acta* **45**: pp 169-175.

Jockusch WJ, Praefcke G J, McMahon H T and Lagnado L (2005) Clathrin-Dependent and Clathrin-Independent Retrieval of Synaptic Vesicles in Retinal Bipolar Cells. *Neuron* **46**: pp 869-878.

Kaksonen M, Toret C P and Drubin D G (2006) Harnessing Actin Dynamics for Clathrin-Mediated Endocytosis. *Nat Rev Mol Cell Biol* **7**: pp 404-414.

Keating DJ, Rychkov G Y and Roberts M L (2001) Oxygen Sensitivity in the Sheep Adrenal Medulla: Role of SK Channels. *Am J Physiol Cell Physiol* **281**: pp C1434-C1441.

Klein DE, Lee A, Frank D W, Marks M S and Lemmon M A (1998) The Pleckstrin Homology Domains of Dynamin Isoforms Require Oligomerization for High Affinity Phosphoinositide Binding. *J Biol Chem* **273**: pp 27725-27733.

Koenig JH and Ikeda K (1989) Disappearance and Reformation of Synaptic Vesicle Membrane Upon Transmitter Release Observed Under Reversible Blockage of Membrane Retrieval. *J Neurosci* **9**: pp 3844-3860.

Larkin JM, Brown M S, Goldstein J L and Anderson R G (1983) Depletion of Intracellular Potassium Arrests Coated Pit Formation and Receptor-Mediated Endocytosis in Fibroblasts. *Cell* **33**: pp 273-285.

Le Roy C and Wrana J L (2005) Clathrin- and Non-Clathrin-Mediated Endocytic Regulation of Cell Signalling. *Nat Rev Mol Cell Biol* **6**: pp 112-126.

Lee A, Frank D W, Marks M S and Lemmon M A (1999) Dominant-Negative Inhibition of Receptor-Mediated Endocytosis by a Dynamin-1 Mutant With a Defective Pleckstrin Homology Domain. *Curr Biol* **9**: pp 261-264.

Lemmon MA (2003) Phosphoinositide Recognition Domains. *Traffic* **4**: pp 201-213.

Lin HC, Barylko B, Achiriloaie M and Albanesi J P (1997) Phosphatidylinositol (4,5)-Bisphosphate-Dependent Activation of Dynamins I and II Lacking the Proline/Arginine-Rich Domains. *J Biol Chem* **272**: pp 25999-26004.

Lindgren CA, Emery D G and Haydon P G (1997) Intracellular Acidification Reversibly Reduces Endocytosis at the Neuromuscular Junction. *J Neurosci* **17**: pp 3074-3084.

Liu JP and Robinson P J (1995) Dynamin and Endocytosis. *Endocr Rev* **16**: pp 590-607.

Marks B and McMahon H T (1998) Calcium Triggers Calcineurin-Dependent Synaptic Vesicle Recycling in Mammalian Nerve Terminals. *Curr Biol* **8**: pp 740-749.

Marks B, Stowell M H, Vallis Y, Mills I G, Gibson A, Hopkins C R and McMahon H T (2001) GTPase Activity of Dynamin and Resulting Conformation Change Are Essential for Endocytosis. *Nature* **410**: pp 231-235.

McNiven MA (1998) Dynamin: a Molecular Motor With Pinchase Action. *Cell* **94**: pp 151-154.

Nicholls DG and Sihra T S (1986) Synaptosomes Possess an Exocytotic Pool of Glutamate. *Nature* **321**: pp 772-773.

Quan A and Robinson P J (2005) Rapid Purification of Native Dynamin I and Colorimetric GTPase Assay. *Methods Enzymol* **404 (Ch 49)**: pp 556-569.

Robinson PJ, Sontag J-M, Liu J P, Fykse E M, Slaughter C, McMahon H T and Südhof T C (1993) Dynamin GTPase Regulated by Protein Kinase C Phosphorylation in Nerve Terminals. *Nature* **365**: pp 163-166.

Roux A, Uyhazi K, Frost A and De Camilli P (2006) GTP-Dependent Twisting of Dynamin Implicates Constriction and Tension in Membrane Fission. *Nature* **441**: pp 528-531.

Salim K, Bottomley M J, Querfurth E, Zvelebil M J, Gout I, Scaife R, Margolis R L, Gigg R, Smith C I E, Driscoll P C, Waterfield M D and Panayotou G (1996) Distinct Specificity in the Recognition of Phosphoinositides by the Pleckstrin Homology Domains of Dynamin and Bruton's Tyrosine Kinase. *EMBO J* **15**: pp 6241-6250.

Scaife R, Venien-Bryan C and Margolis R L (1998) Dual Function C-Terminal Domain of Dynamin-1: Modulation of Self-Assembly by Interaction of the Assembly Site With SH3 Domains. *Biochemistry* **37**: pp 17673-17679.

Schreier S, Malheiros S V and de Paula E (2000) Surface Active Drugs: Self-Association and Interaction With Membranes and Surfactants. Physicochemical and Biological Aspects. *Biochim Biophys Acta* **1508**: pp 210-234.

Scurlock JE and Curtis B M (1981) Tetraethylammonium Derivatives: Ultralong-Acting Local Anesthetics? *Anesthesiology* **54**: pp 265-269.

Sheff D, Pelletier L, O'Connell C B, Warren G and Mellman I (2002) Transferrin Receptor Recycling in the Absence of Perinuclear Recycling Endosomes. *J Cell Biol* **156**: pp 797-804.

Stowell MH, Marks B, Wigge P and McMahon H T (1999) Nucleotide-Dependent Conformational Changes in Dynamin: Evidence for a Mechanochemical Molecular Spring. *Nat Cell Biol* **1**: pp 27-32.

Tan TC, Valova V A, Malladi C S, Graham M E, Berven L A, Jupp O J, Hansra G, McClure S J, Sarcevic B, Boadle R A, Larsen M R, Cousin M A and Robinson P J (2003) Cdk5 Is Essential for Synaptic Vesicle Endocytosis. *Nat Cell Biol* **5**: pp 701-710.

Trowbridge IS, Collawn J F and Hopkins C R (1993) Signal-Dependent Membrane Protein Trafficking in the Endocytic Pathway. *Annu Rev Cell Dev Biol* **9**: pp 129-161.

Vallis Y, Wigge P, Marks B, Evans P R and McMahon H T (1999) Importance of the Pleckstrin Homology Domain of Dynamin in Clathrin-Mediated Endocytosis. *Curr Biol* **9**: pp 257-260.

van der Bliek AM, Redelmeier T E, Damke H, Tisdale E J, Meyerowitz E M and Schmid S L (1993) Mutations in Human Dynamin Block an Intermediate Stage in Coated Vesicle Formation. *J Cell Biol* **122**: pp 553-563.

Van Veldhoven PP and Mannaerts G P (1987) Inorganic and Organic Phosphate Measurements in the Nanomolar Range. *Anal Biochem* **161**: pp 45-48.

Wang L-H, Rothberg K G and Anderson R G (1993) Mis-Assembly of Clathrin Lattices on Endosomes Reveals a Regulatory Switch for Coated Pit Formation. *J Cell Biol* **123**: pp 1107-1117.

Yan Z, Chi P, Bibb J A, Ryan T A and Greengard P (2002) Roscovitine: a Novel Regulator of P/Q-Type Calcium Channels and Transmitter Release in Central Neurons. *J Physiol* **540**: pp 761-770.

Zheng J, Cahill S M, Lemmons M A, Fushman D, Schlessinger J, Cowburn D and Lemmon M A (1996) Identification of the Binding Site for Acidic Phospholipids on the PH Domains of Dynamin: Implications for Stimulation of GTPase Activity. *J Mol Biol* **255**: pp 14-21.

FOOTNOTES

This work was supported by grants from the National Health and Medical Research Council

(Australia) and The Wellcome Trust (Ref: 062841).

Molecular Pharmacology Fast Forward. Published on August 16, 2007 as DOI: 10.1124/mol.107.034207
This article has not been copyedited and formatted. The final version may differ from this version.

LEGENDS FOR FIGURES

Figure 1. *MiTMAB inhibits the GTPase activity of dynamin I and targets the PH domain*. (A) The GTPase activity of native sheep brain dynamin I (20 nM) was determined in the presence of different concentrations of MiTMAB. Phospholipid (PS, 1.2 μM) stimulated activity (filled symbols) was measured. The graph is representative of 3 independent experiments. Results are mean (triplicates) with a 95% confidence interval (CI) (dashed line) for each experiment. (B-C) The effect of MiTMAB on basal and PS (1.2 μM) stimulated dynamin I (wild-type (WT), panel B) and dynamin I-ΔPH (panel C) GTPase activity was compared in the absence or presence of 10 μM and 30 μM MiTMAB. The values are the means ± SEM, n=3. Although WT and ΔPH dynamin were both used at 20 nM in this assay, the maximal activity of was ΔPH was about half that of WT because the recombinant ΔPH lacks the cooperative lipid-mediated assembly enhanced GTPase activity. (D) *In vitro* phospholipid binding; WT dynamin was incubated with phospholipid in the absence and presence of MiTMAB at the concentrations indicated. The Coomassie stained polyacrylamide gel is a representative image of 3 independent experiments with similar results.

Figure 2. *MiTMAB is a competitive inhibitor with PS and non-competitive with GTP.* The effect of MiTMAB on Michaelis-Menten (A) and Lineweaver-Burke (B) plots of the GTPase activity of WT dynamin I (20 nM) with increasing concentrations of GTP and a fixed concentration of PS (12.7 μM). Michaelis-Menten (C) and Lineweaver-Burke (D) plots of the GTPase activity of WT dynamin I in the absence and presence of indicated concentrations of MiTMAB at increasing concentrations of PS liposomes and a fixed concentration of GTP

Molecular Pharmacology Fast Forward. Published on August 16, 2007 as DOI: 10.1124/mol.107.034207
This article has not been copyedited and formatted. The final version may differ from this version.

(300 μM). (E) The Michaelis-Menten constants V_{max}, K_m and K_i with a 95% CI were calculated from triplicate samples performed during a single experiment. All results are representative of at least 2 independent experiments.

Figure 3. *MiTMAB blocks internalization of Tf-TxR and EGF-A488 in non-neuronal cells.* HeLa cells were preincubated with vehicle only (A-C) or MiTMAB (D-F (30 or 100 μM)) for 10 min. Cells were then incubated with Tf-TxR (A, D and G) and EGF-A488 (B, E and H) for 15 min at 37°C, acid washed, fixed and internalized Tf-TxR and EGF-A488 was detected by fluorescence microscopy. Nuclei were stained blue with DAPI to show the position of the cells (C, F, and I). (J, K, and L) MiTMAB is a reversible inhibitor. A431 cells were preincubated with vehicle only (J) or 30 μM MiTMAB (K-L) for 10 min and then incubated with EGF-A488 for 10 min. Cells treated as in panel K were washed for 30 min without MiTMAB and then incubated with EGF-A488 for 15 min. Images are representative of 2 independent experiments. (M and O) Quantitative analysis of EGF-A488 endocytosis in COS-7 cells in the presence of different concentrations of the inhibitors. Data is mean fluorescence as a percent of fluorescence in control cells (triplicate determinations on approximately 1,200 cells each) ± SEM. The results are representative of 3 independent experiments. Endocytosis in control cells (no drug, DMSO-treated) is expressed as 100%. (K and M) IC_{50} values ± 95% CI for the data in panel J and L respectively.

Figure 4. *MiTMAB does not block Tf and EGF binding and EGFR activation.*
(A) Tf binding assay. COS-7 cells were either preincubated with DMSO (control) or MiTMAB (30 μM for 10 min) at 37°C then incubated for different times with biotinylated-Tf (10 μg/ml) on ice for Tf cell surface binding. Cell lysates were analyzed by Western blot and

probed with avidin-HRP to detect the amount of biotinylated-Tf in cell lysates. Blots were quantitated using densitometry and the intensity (arbitrary units) of the biotinylated-Tf was normalized against an endogenous biotinylated protein on the blots and the average of the range of values was plotted. Error bars indicate the range of values (n=2). (B-E) Surface EGF binding assay. A431 cells were preincubated with DMSO (control) (B and C) or 30 μM MiTMAB (D and E) for 10 min at 37°C then placed on ice and incubated with EGF-A488 (600 ng/ml) for 30 min, fixed in 4% PFA at room temperature (22°C) and counterstained with DAPI. Images are maximum projection images generated from 3D deconvolution of Z stack images and are representative of 2 independent experiments. (F) Western blots of EGFR phosphotyrosine (pEGFR) and total endogenous EGFR levels in A431 cell lysates preincubated without (control) or with MiTMAB, OcTMAB, or genistein (negative control, each drug at 30 μM) for 10 min at 37°C and then stimulated with EGF (100 ng/ml). (G) Densitometry analysis of the blots. The intensity of the EGFR phosphotyrosine signals were normalized to their respective total EGFR signals and then expressed as a relative intensity (%) of the EGF-stimulated control sample. Error bars indicate the range of values (n=2).

Figure 5. *MiTMAB prevents PH domain localization on plasma membranes.*
HeLa cells were transfected with GFP-dyn I-PH domain (A-B) and then incubated with 30 μM MiTMAB (C-D) or 30 μM myristic acid (E-F) at 37°C for 30 min. The distribution of GFP-dyn I-PH domain was detected by confocal fluorescence microscopy. The top and middle panels are representative images of single cells from 2 independent experiments. While most of the expressed protein was cytosolic, a significant membrane distribution is evident in all control cells. Boxes indicate regions of the plasma membrane that are shown at higher magnification in the lower panels. The same results were obtained in 3 independent

experiments and the scale bar = 10 μm (A-F).

Figure 6. *MiTMAB inhibits exocytosis and Ca^{2+} entry in chromaffin cells.*

(A-B) Carbon fiber amperometry was used to measure catecholamine release (shown as spikes) from single rat adrenal chromaffin cells induced by two pulses of high KCl (70 mM) bath solution for 1 min (S1 and S2). Double sloped lines at the bottom of the traces indicate a break in recording. Following the first stimulation, cells were washed for 5 min and then exposed for 10 min to a solution containing either MiTMAB (30 μM in 0.3% DMSO, panel B) or an equivalent volume of DMSO in bath solution (A). The results are summarized for both the number of secretory events (C) and the total amount of charge released (D) in 1 min (n = 9 for both control and MiTMAB-treated cells). The results for DMSO or MiTMAB alone are over a 10 min period and represent all recorded cells. (E) Fluorescence of cells loaded with Fluo-3 increased significantly upon exposure to high KCl (70 mM) solution (the period of stimulation is indicated by a solid bar). The effect of preincubation with MiTMAB for 1 or 10 min is shown. (F) Quantitative analysis of the Ca^{2+} results such as in panel e. The absolute change in fluorescence due to Ca^{2+}-influx ($\triangle F$) is shown as mean ± SD (n = 14, 10 and 14 cells for each column left to right). ** indicates significantly less than S1 value ($p<0.001$).

Figure 7. *MiTMAB inhibits SVE and not exocytosis in synaptosomes*.

(A) Synaptosomes were preincubated with MiTMAB (30 μM) for 10 min prior to stimulation with 30 mM KCl. The effect on SV exocytosis (calcium-dependent glutamate release) is displayed in the absence (control) or presence of MiTMAB. (B) Synaptosomes were incubated with or without MiTMAB (30 μM) for 10 min, then loaded with FM2-10 using a 2

min KCl stimulus, and the extent of loading (endocytosis) was estimated with a subsequent unloading stimulus to release the accumulated dye (Cousin and Robinson, 2000). Endocytosis (calcium-dependent uptake and release of FM2-10) in the absence or presence of MiTMAB is shown as the decrease in fluorescence. The bar in A and B denotes the presence of KCl. (C) Retrieval efficiency (endocytosis divided by exocytosis) was significantly inhibited (* $p<0.05$, $n=5 \pm$ SEM), indicating a specific block in SVE. (D-I) Effect of MiTMAB on synaptosome morphology. Synaptosomes were treated with vehicle alone (D-E) or MiTMAB (30 μM for 5 min) (F-I), then incubated in control buffer, ie at "rest" (D and F) or were depolarized with 30 mM KCl for 2 min (panels E and G-I). Synaptosomes were pelleted and fixed for electron microscopy. Images are representative of two independent experiments. The scale bars = 200 nm.

Molecular Pharmacology Fast Forward. Published on August 16, 2007 as DOI: 10.1124/mol.107.034207
This article has not been copyedited and formatted. The final version may differ from this version.

TABLES

Table 1. Inhibition of dynamin I GTPase activity by long chain acids, amines and ammonium salts.

	Compound	Structure	Molecular Weight	IC_{50} (μM)
1	Myristic acid	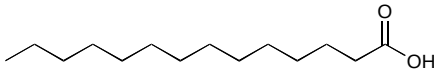	228.4	>300
2	2-(dimethyl amino) ethyl myristate	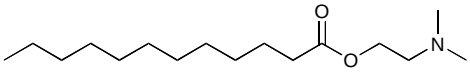	299.5	9.2 ± 0.96
3	Tetradecylamine	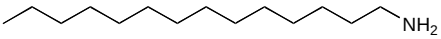	213.4	6.5 ± 1.0
4	Dodecyl trimethyl ammonium bromide (DoTMAB)	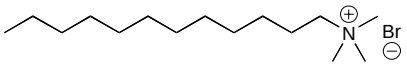	308.4	9.0 ± 1.4
5	Myristyl trimethyl ammonium bromide (MiTMAB)	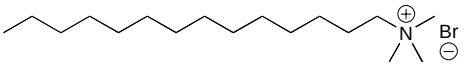	336.4	3.1 ± 0.2
6	Octadecyl trimethyl ammonium bromide (OcTMAB)	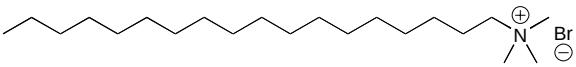	392.5	1.9 ± 0.24

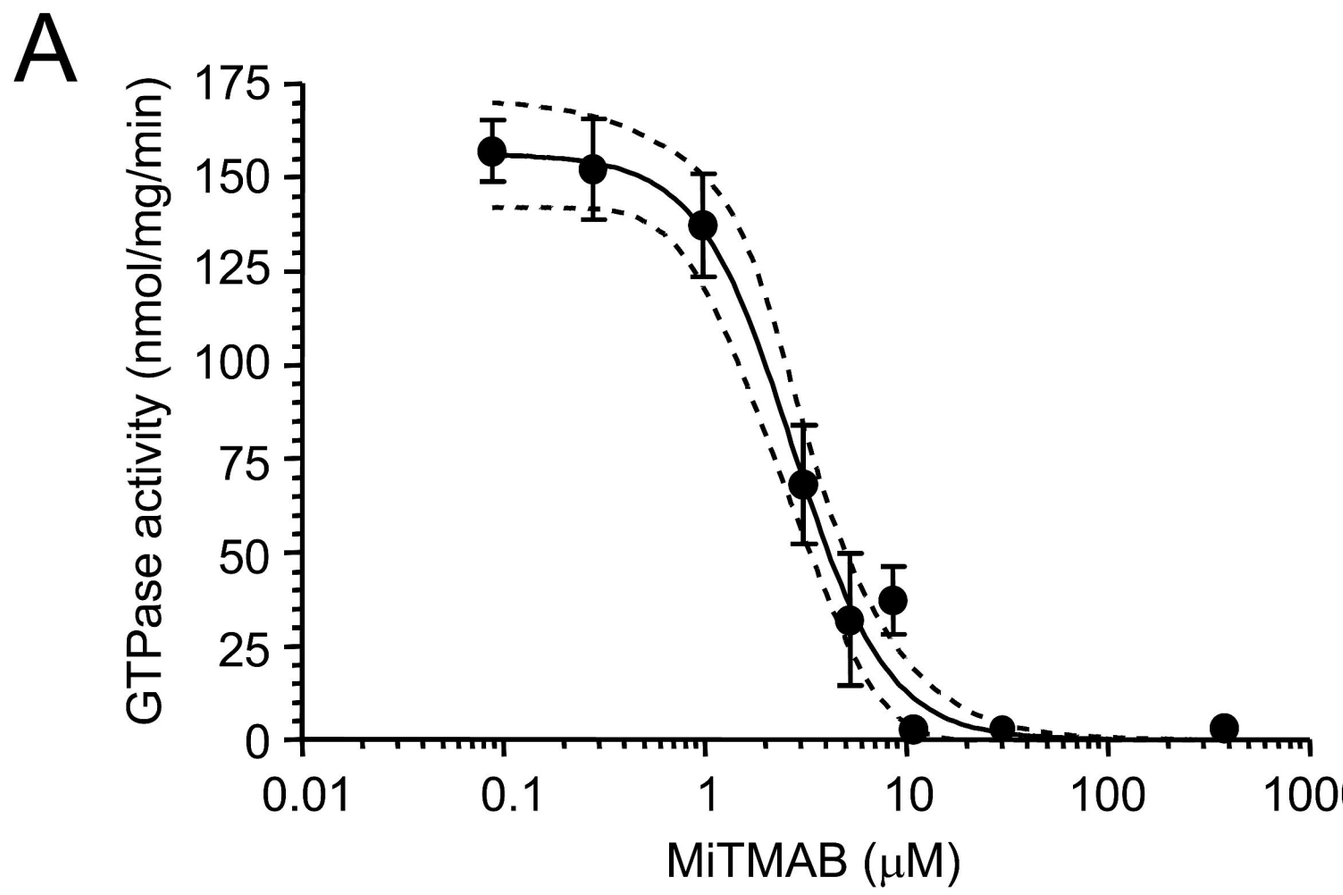

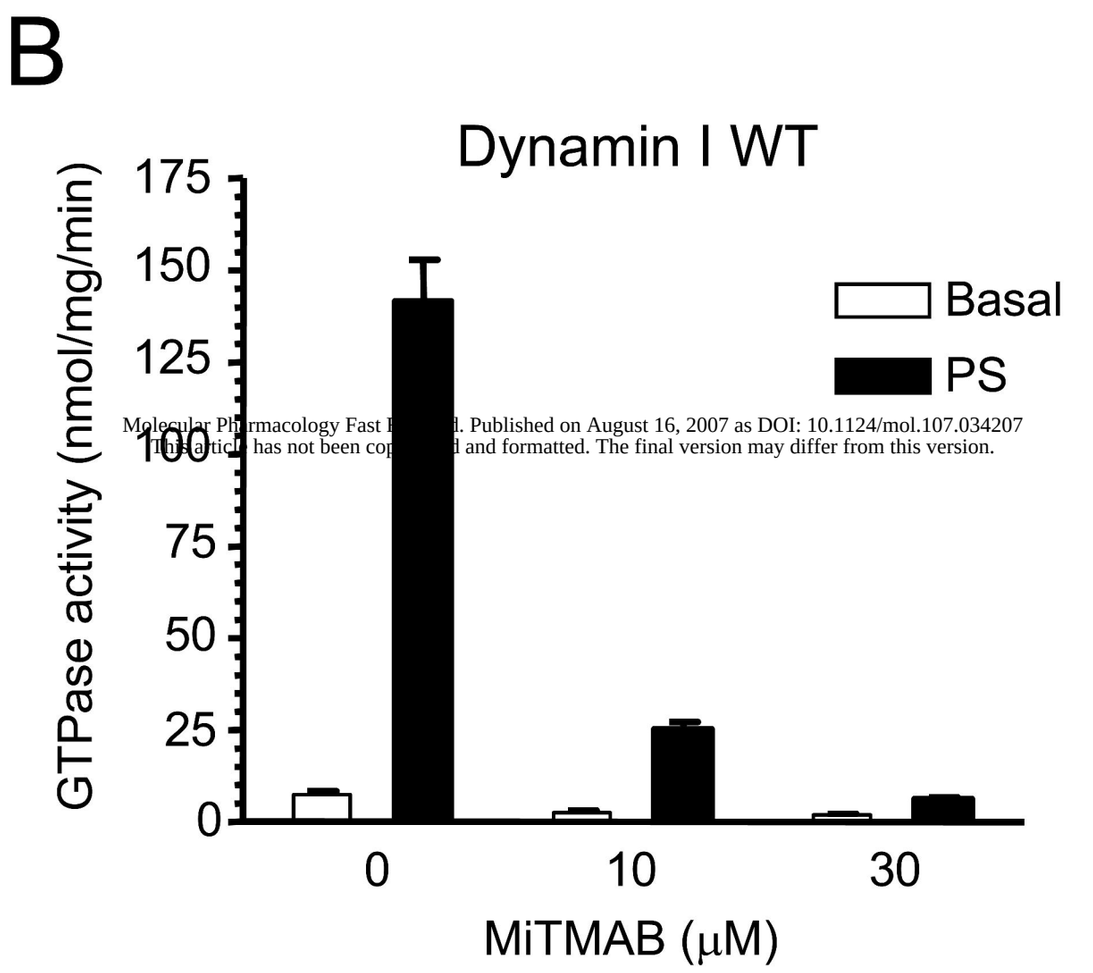

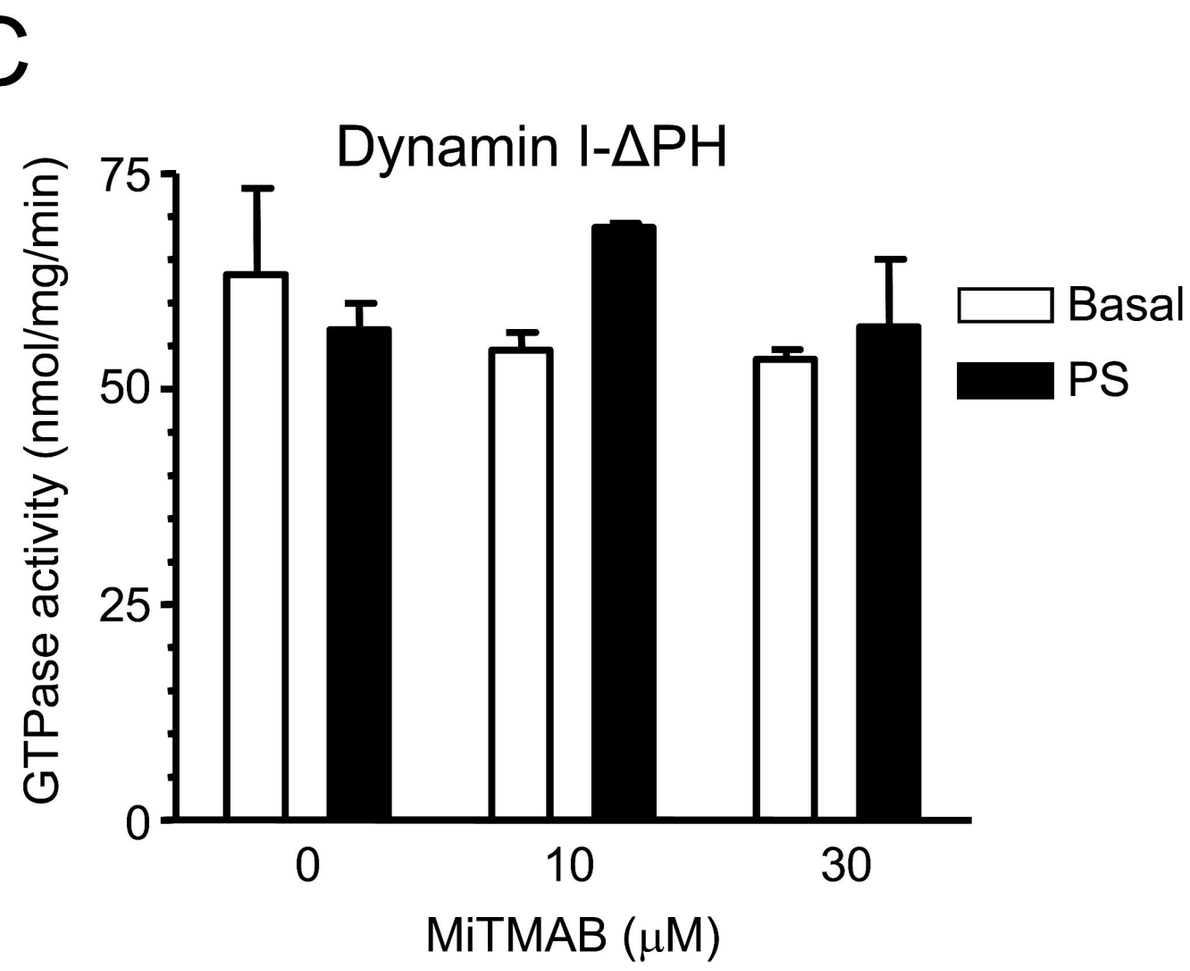

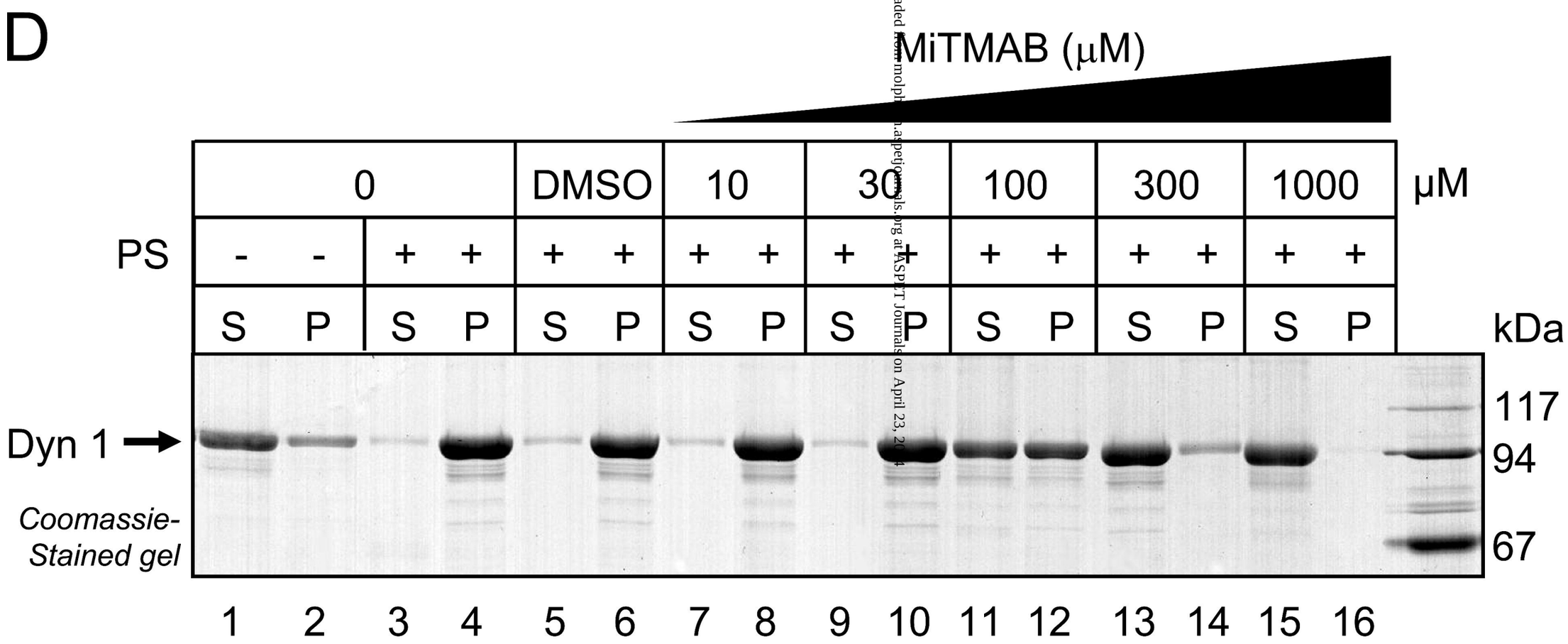

Figure 1.

A

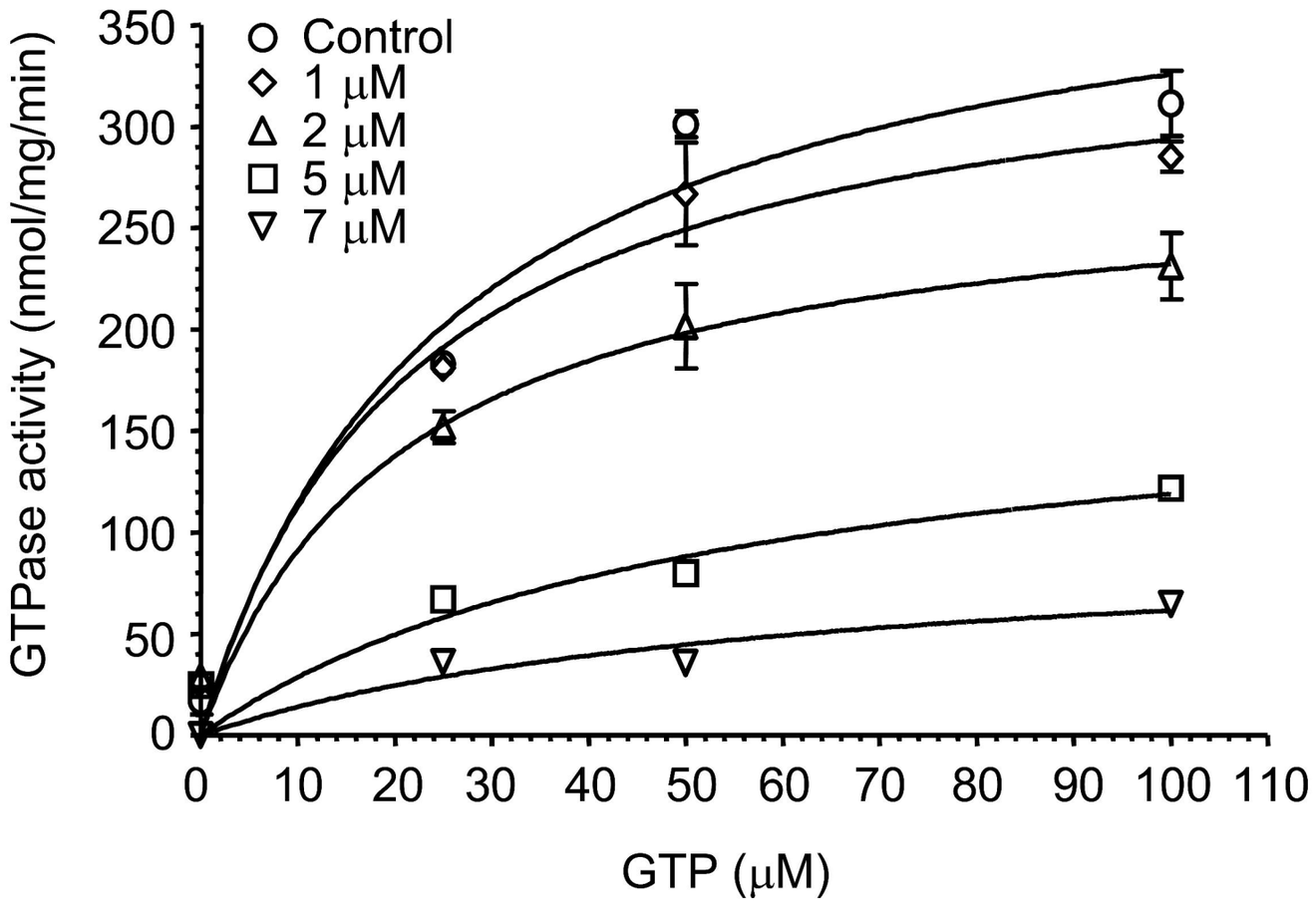

B

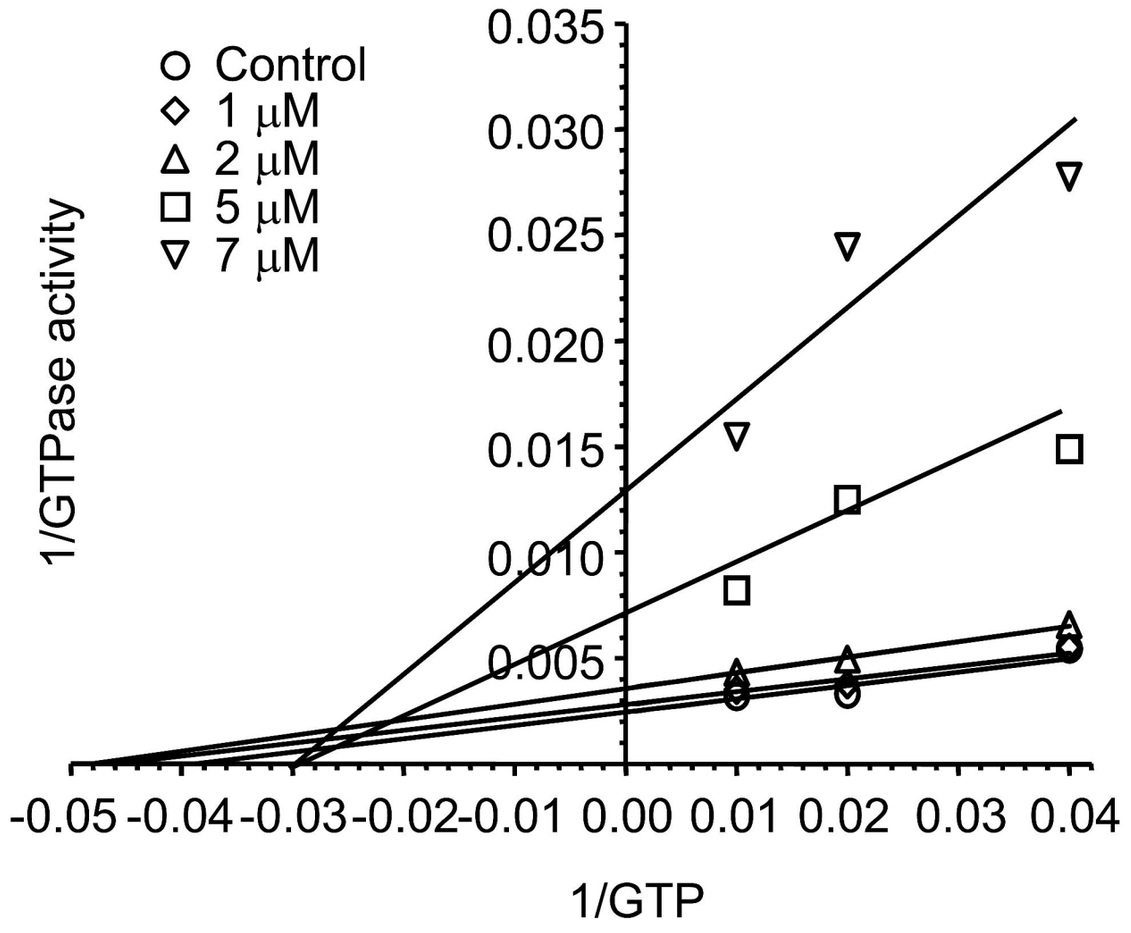

C

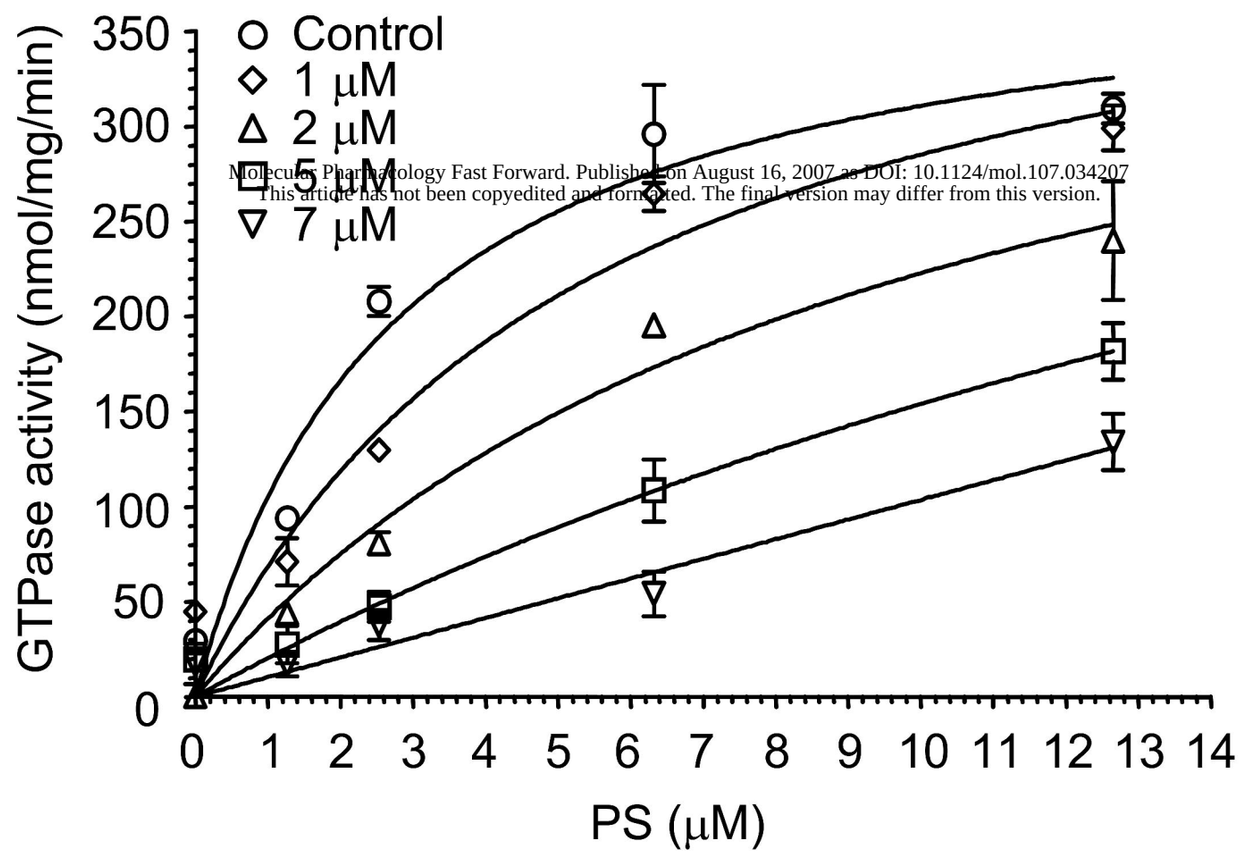

D

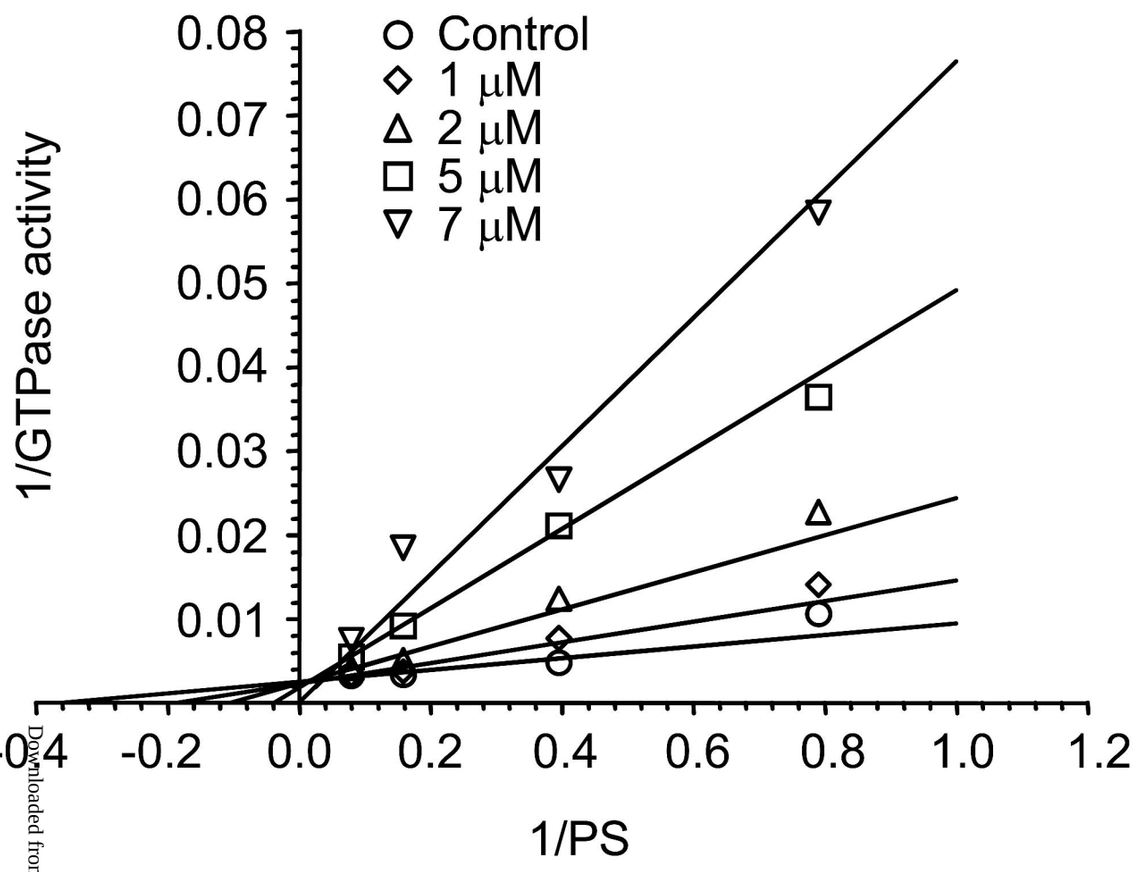

E

Substrate	Constant	Value
GTP	V_{max}	430 ± 57 nmol/mg/min
	K_m	20.9 ± 10.0 μM
PS	V_{max}	428 ± 40 nmol/mg/min
	K_m	3.1 ± 0.87 μM
	K_i	940 ± 25 nM

Figure 2.

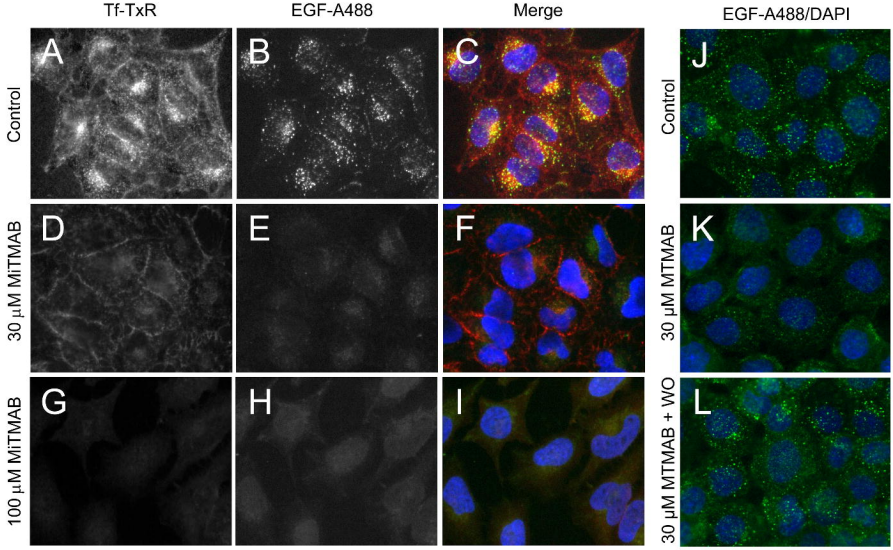

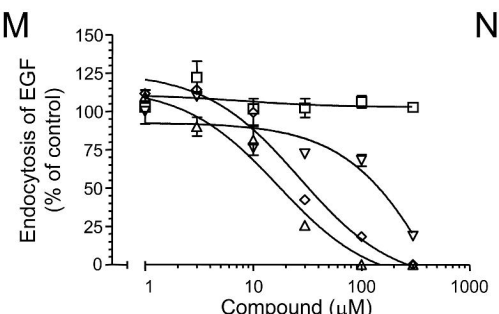

N

	Compound	IC_{50} (μM)
□	Myristic acid	≥ 300
▽	DoTMAB	160 ± 48
◇	MiTMAB	20.9 ± 3.2
△	OcTMAB	16.0 ± 4.2

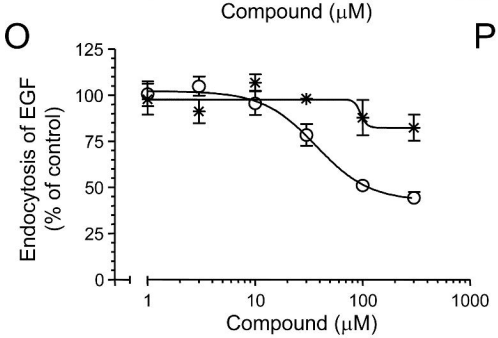

P

	Compound	IC_{50} (μM)
✳	2-(dimethylamino) ethyl myristate	≥ 300
○	Tetradecylamine	37.2 ± 21

Figure 3.

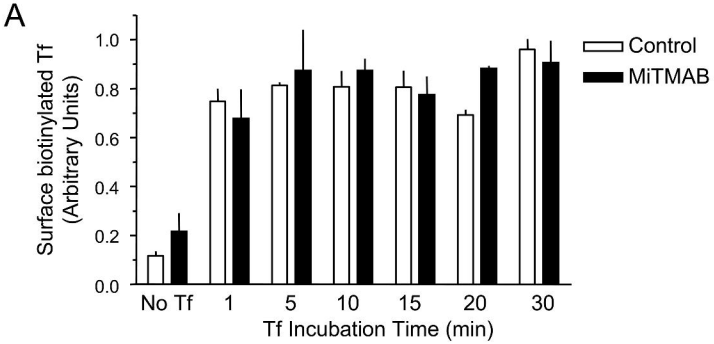
A
Surface biotinylated Tf
(Arbitrary Units)
1.0
0.8
0.6
0.4
0.2
0.0
Control
MiTMAB
No Tf
1
5
10
15
20
30
Tf Incubation Time (min)

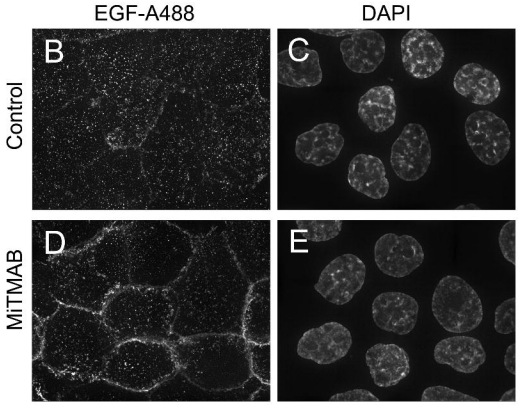
EGF-A488
DAPI
Control
MiTMAB
B
C
D
E

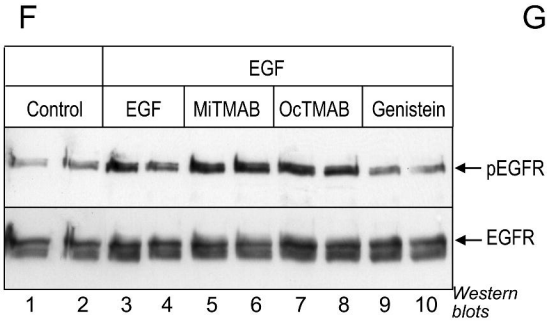
F
EGF
Control
EGF
MiTMAB
OcTMAB
Genistein
pEGFR
EGFR
1
2
3
4
5
6
7
8
9
10
Western blots

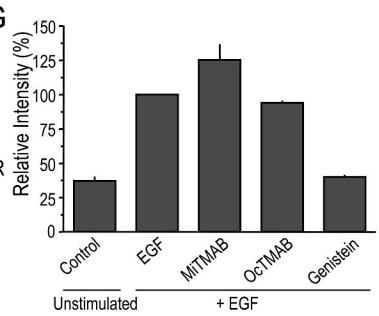
G
Relative Intensity (%)
150
125
100
75
50
25
0
Control
EGF
MiTMAB
OcTMAB
Genistein
Unstimulated
+ EGF

Figure 4.

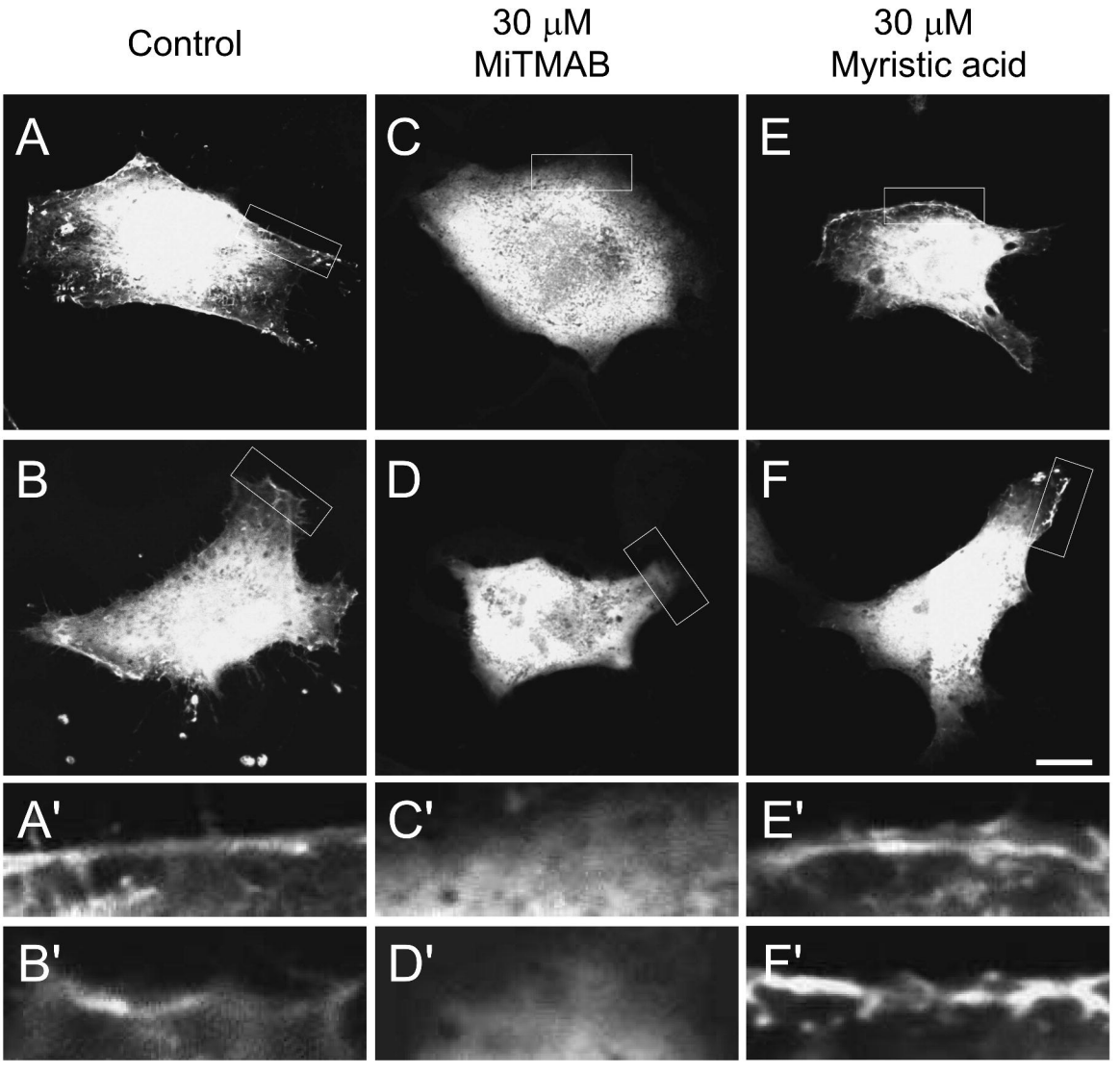

Figure 5

Molecular Pharmacology Fast Forward. Published on August 16, 2007 as DOI: 10.1124/mol.107.034207
This article has not been copyedited and formatted. The final version may differ from this version.

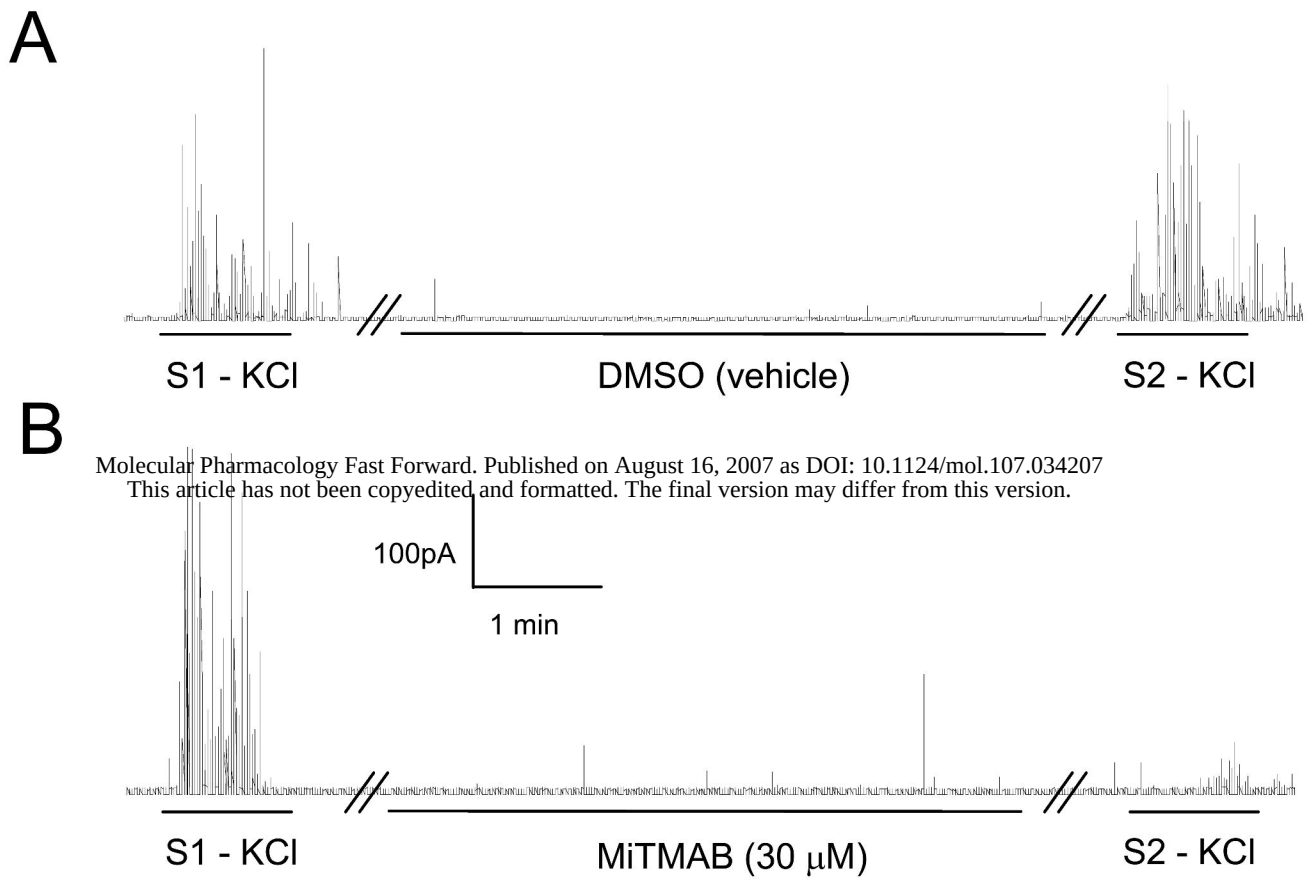

Figure 6.

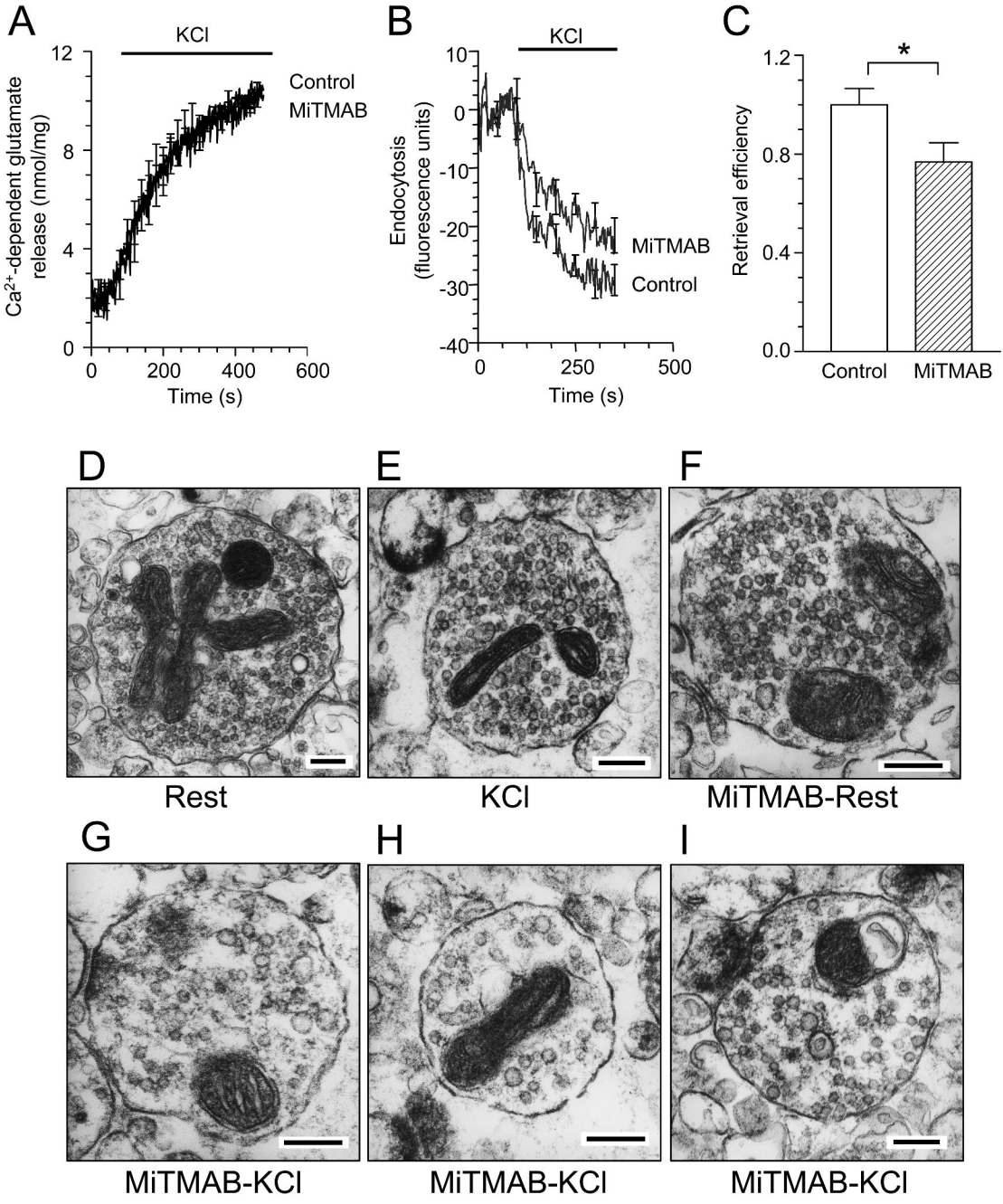
A
KCl
Control
MiTMAB
Ca^{2+}-dependent glutamate release (nmol/mg)
Time (s)
B
KCl
MiTMAB
Control
Endocytosis (fluorescence units)
Time (s)
C
Retrieval efficiency
Control
MiTMAB
D
E
F
Rest
KCl
MiTMAB-Rest
G
H
I
MiTMAB-KCl
MiTMAB-KCl
MiTMAB-KCl

Figure 7.